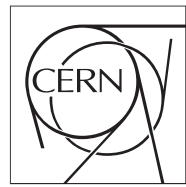
**The Compact Muon Solenoid Experiment**

CMS Note

Mailing address: CMS CERN, CH-1211 GENEVA 23, Switzerland



2013/09/30

Projected Performance of an Upgraded CMS Detector at the LHC and HL-LHC: Contribution to the Snowmass Process

CMS Collaboration

Abstract

The physics reach of the CMS detector achievable with $300(0) \text{ fb}^{-1}$ of proton-proton collisions recorded at $\sqrt{s} = 14 \text{ TeV}$ is presented. Ultimate precision on measurements of Higgs boson properties, top quark physics, and electroweak processes are discussed, as well as the discovery potential for new particles beyond the standard model. In addition, the potential for future heavy ion physics is presented. This document has been submitted as a white paper to the Snowmass process, an exercise initiated by the American Physical Society's Division of Particles and Fields to assess the long-term physics aspirations of the US high energy physics community.

1 Introduction

The Division of Particles and Fields of the American Physical Society has initiated a Snowmass process [1] to assess the long-term physics aspirations of the US high energy physics community. This exercise has been organized into several “frontiers,” of which the primary one relevant to the Compact Muon Solenoid (CMS) collaboration is the Energy Frontier. The CMS Collaboration also performs measurements that are relevant to the Cosmic and Intensity frontiers, and there are frontiers devoted to forefront advances in Instrumentation and Computing that impact directly on the future capabilities of the detector. The high energy physics landscape is studied with respect to future capabilities provided by both accelerator-based facilities and detector facilities distinct from accelerators, which have been assessed by the Frontier Capabilities working group. Of the future accelerator options currently under study, the Large Hadron Collider (LHC) is the only facility currently operating. In this document we summarize the physics potential of the upgraded CMS detector operating during the future LHC running planned over the next two decades.

The LHC has performed flawlessly since initiating high-energy pp collisions at $\sqrt{s} = 7\text{ TeV}$ in early 2010, delivering 30 fb^{-1} of data to CMS during the past three years (see Fig. 1). In 2012 the energy was raised to a new record of 4 TeV per beam, while the instantaneous luminosity exceeded $7 \times 10^{33}\text{ cm}^{-2}\text{ s}^{-1}$ and the average number of interactions per pp crossing (pile-up) reached 21. The CMS detector was able to operate effectively in this high-occupancy environment, recording 27 fb^{-1} of high-quality pp data with efficiency in excess of 90%. This data has been used to discover a Higgs boson, to extend the search for particles beyond the standard model (SM) to the multi-TeV range, and to make measurements of electroweak processes and top-quark properties with a precision exceeding that achieved by the Tevatron. In addition, CMS has collected $150\text{ }\mu\text{b}^{-1}$ of lead-lead and 31 nb^{-1} of proton-lead collisions that have fundamentally expanded our understanding of heavy ion physics.

Currently, the LHC is in the middle of its first long shutdown (LS1) in order to prepare for running at $\sqrt{s} = 13\text{ TeV}$ in 2015, on the way to the design energy of 14 TeV . The bunch spacing will most likely be reduced to 25 ns, the luminosity will reach the design value ($10^{34}\text{ cm}^{-2}\text{ s}^{-1}$) with 25 pile-up interactions, and the goal will be to integrate 300 fb^{-1} of pp data by the end of 2021. A second long shutdown (LS2) in 2018 will be used to upgrade the detectors for running at double the design luminosity and an average pile-up of 50. The next phase of planned LHC operation, referred to as the High Luminosity LHC (HL-LHC), will begin with the third long shutdown (LS3) in the period 2022-2023, where the machine and detectors will be upgraded to allow for pp running at a luminosity of $5 \times 10^{34}\text{ cm}^{-2}\text{ s}^{-1}$ and an average pile-up of 128, with the goal of eventually accumulating 3000 fb^{-1} .

The increase in LHC beam energy will have a significant impact on the physics reach of CMS beyond that gained by accumulating 10 or 100 times more data. In addition to the increase in production cross section, a multi-TeV particle produced via gluon fusion will see an increase in the parton luminosity by one or two orders of magnitude relative to 7 TeV collisions (Fig. 1). The jump in energy will lead to a doubling of the mass reach for discovery of new particles early in the next run, while enabling precision measurements of Higgs boson properties and SM processes that will either help to elucidate the nature of newly discovered particles or exclude a large set of possible alternatives to the standard model.

The purpose of this document is to summarize, in the context of the Snowmass process, the future physics potential of the CMS detector at the LHC operating with protons and heavy ions at design energy and luminosities up to $5 \times 10^{34}\text{ cm}^{-2}\text{ s}^{-1}$. The methodology used to make

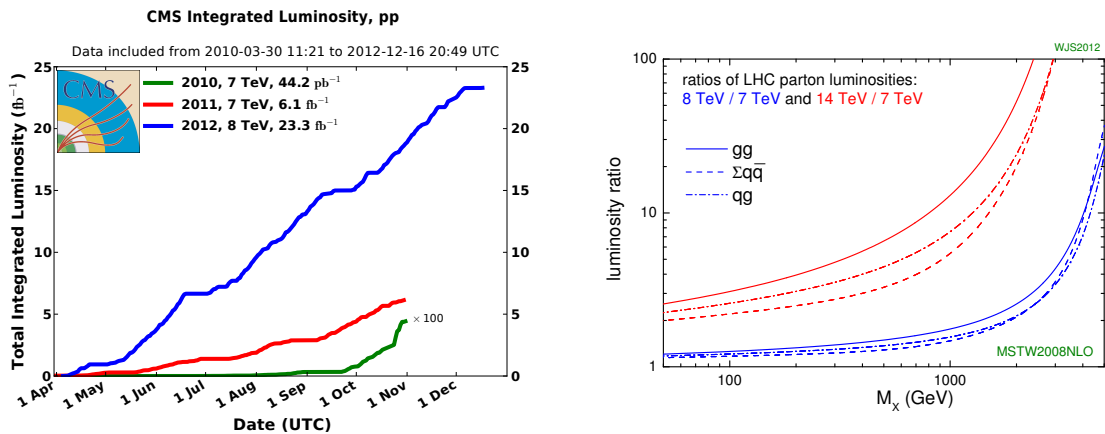


Figure 1: Left: LHC integrated luminosity delivered to CMS during the 2010 (green), 2011 (red), and 2012 (blue) running periods. Right: ratio of parton luminosities at the LHC for center-of-mass energies of 8 and 14 TeV relative to 7 TeV. Luminosities are shown separately for processes initiated by gg , qg , and qq collisions [2].

projections is based on the assumption that the planned upgrades of the CMS detector will achieve the goal of mitigating the increased radiation damage and complications arising from higher luminosity and higher pile-up. With this primary assumption, existing public results based on current data are extrapolated to higher energy and luminosities. In most cases, the analyses are assumed to be unchanged, which is a conservative assumption given the fact that all analyses will be reoptimized to maximally exploit the higher energy and luminosity. This white paper updates and extends the conclusions summarized in the CMS report [3] submitted to the European Strategy Preparatory Group in October, 2012, and is organized as follows. Section 2 summarizes the current physics landscape at the Energy Frontier, while Sec. 3 describes the CMS upgrade plans for LHC Phases 1 and 2. Section 4 presents the projected measurement sensitivity of Higgs boson properties, while Secs. 5 and 6 summarize the discovery reach for supersymmetry and exotic resonances, respectively. Sections 7-9 summarize the physics potential for top-quark, electroweak, and heavy-ion physics, respectively, and concluding remarks are given in Sec. 10.

2 LHC Physics Landscape (2013)

By the end of the 2010 LHC data-taking period at 7 TeV, all of the SM particles had been rediscovered by both CMS and ATLAS (neutrinos through missing energy). By the end of 2011 the search for the SM Higgs boson had excluded a wide range of masses, leaving only a narrow allowed region around 125 GeV where an indication of a signal had appeared. Increasingly precise measurements of top quark and electroweak processes continued to confirm the standard model, and the absence of any signals in the search for new particles beyond the standard model (BSM) motivated a new class of simplified supersymmetric (SUSY) models to test in the 8 TeV data.

In July of 2012 the landscape changed fundamentally when the ATLAS [4] and CMS [5] collaborations announced the discovery of a new particle with a mass near 125 GeV possessing properties consistent with that of the long-sought Higgs boson. Since that time, both experiments have analyzed the full 8 TeV dataset, comprising approximately 20 fb^{-1} of proton-proton collision data, and reported preliminary results for the main boson decay channels [6–9]. CMS

has also shown preliminary results on the full dataset for the primary fermion decay channels [10, 11], where an indication of a signal has started to materialize, while ATLAS has presented preliminary results on the full dataset in the bottom-quark channel [12]. All of the main production channels accessible at the LHC have now been investigated experimentally, including gluon fusion, vector-boson fusion, and associated production with vector bosons and top quarks. Within the existing experimental and theoretical precision, all measurements of the coupling of the new boson to photons, W and Z bosons, tau leptons, and bottom quarks are consistent with the expected couplings of the SM Higgs boson [13, 14]. In addition, the hypothesis that the new boson is a scalar has been tested against alternative spin-parity hypotheses by CMS [15] and ATLAS [16], with results disfavoring all but the SM prediction. One year after the initial discovery it is now clear that this particle is a Higgs boson, but whether it is the single particle predicted in the standard model, or only one of many Higgs bosons, remains a central open question. This question will be the focus of intense research in particle physics for the foreseeable future.

As of the time of writing, no new particles have been discovered apart from a Higgs boson. Exclusions for gluinos are now extended up to ~ 1.3 TeV, while first- and second-generation squarks are excluded up to ~ 0.8 TeV assuming an eightfold squark-mass degeneracy. Third-generation squarks are excluded up to ~ 650 GeV, and electroweak gauginos are excluded up to ~ 300 GeV when sleptons are decoupled. The search for new gauge bosons with SM couplings has yielded lower limits of 3 TeV, while more exotic models such as black holes and string resonances are excluded up to 5 TeV. The increase in energy of the LHC will have a significant effect on the discovery reach for new particles, and the full exploitation of this new phase space will be a primary goal of the next run after LS1.

Electroweak processes, including diboson production and W and Z production in association with up to four jets, have been measured with increasing precision and no deviations from the SM predictions have been found. Such processes represent important reducible and irreducible backgrounds to Higgs boson production and will be critical to improve upon in future running to achieve the target precision on its properties. CMS has measured the top-quark mass to a precision of better than 1%, while the uncertainties on the top-pair and single-top cross sections in the t-channel are less than 10%. Searches for new particles produced in association with, or decaying to, top quarks have so far resulted in only exclusion limits.

Given this current landscape, the physics goals of the future LHC running are clear. The properties of the new boson must be measured to the highest achievable precision, including the Higgs self-coupling, while additional Higgs bosons and exotic decays must be either found or excluded. At the same time, the existence of a Higgs boson intensifies the search for supersymmetric particles, and the upgraded CMS detector must be able to simultaneously trigger on electroweak-scale physics while remaining sensitive to broadband particle searches in the multi-TeV regime. The precision of top and electroweak measurements must continue to improve, both as a way to reduce the systematic uncertainty on Higgs boson measurements and as potential probes of subtle new physics effects. The CMS upgrades are designed to enable this physics by not only mitigating the effects of radiation damage and higher luminosity, but by improving the performance of the detector in key areas relative to the existing performance at 8 TeV.

3 CMS Upgrades

A number of modifications to the LHC experiments are required to deal with the increased instantaneous luminosity that the LHC will deliver in Run 2 and beyond. The improvements

to the LHC experiments that will be installed through the period encompassing LS1 and LS2 are referred to as “Phase 1” upgrades, while those planned for installation in LS3 are referred to as “Phase 2.” This section describes the CMS upgrade program and its goals.

3.1 Phase 1 Upgrades to the CMS Experiment

For the CMS experiment, the planned Phase 1 upgrades involve the innermost tracking detector composed of silicon pixels, the hadron calorimeter, and the first level of the CMS trigger. The pixel detector will be replaced with an improved device that adds a fourth layer to its design. In addition to improving the overall quality and robustness of track reconstruction, the upgraded pixel system will provide substantially improved b-tagging capability. The readout of the hadron calorimeter will be replaced to exploit newly available silicon phototransducer technology. In addition to addressing shortcomings of the existing readout system, this will allow for longitudinal segmentation of the calorimeter, allowing for improved “particle flow” reconstruction in high-occupancy events. The L1 Trigger system will be upgraded to allow use of the full granularity of the calorimeter. The upgraded system will also permit the combination of cluster information from the different muon subsystems directly at the L1 muon track reconstruction level, as well as improved capability to exploit the intrinsic cluster position resolution.

Planning for each of these upgrades is at an advanced stage, with the technical description and expected performance of these upgraded detectors documented in detail in Technical Design Reports approved by the LHCC [17–19]. Salient aspects of these details with respect to the CMS physics program are summarized in the following sections, wherein the vital necessity of each component of the Phase 1 upgrades is demonstrated.

3.1.1 Pixel Detector Upgrade

The CMS pixel detector has efficiently recorded data since the first LHC collisions in 2009. It provides high track reconstruction efficiency and precise measurement of track origin, as needed for online event selection and offline physics analyses. CMS analyses are based on the particle flow technique to provide a globally optimized reconstruction of physics objects (isolated leptons and photons, jets and missing transverse energy). With the 2012 LHC dataset, it has been observed that the pixel performance is essential to mitigate the effect of numerous interactions in the same bunch crossing to maintain efficient identification of all physics objects. This performance, however, is not maintainable with the current pixel detector when LHC beam conditions significantly exceed their original design specifications and it must be replaced with a new device.

The performance of the present pixel detector at high luminosity is limited by reduced hit efficiency in the readout chip for the innermost layers, and bandwidth limitations in the optical links. A new detector has been designed that overcomes these limitations, improves the track impact parameter resolution, and reduces the effect of particle interactions in the detector materials. It contains an optimized configuration for 4-hit coverage over the pseudo-rapidity range up to $\eta = 2.5$, with 4 layers in the barrel and 3 disks in the end-caps, a new read-out chip (ROC) architecture with high hit rate capability, a significantly reduced material budget, new optical links and data acquisition system with a higher output bandwidth, and a modified power supply system using DC-DC converters on the detector to reduce power losses. The new pixel detector, with these characteristics, will survive the radiation dose expected through LS3, with a single exchange of the innermost barrel layer at mid-term.

The overall configuration of the new detector is shown in Fig. 2. The first barrel layer is moved

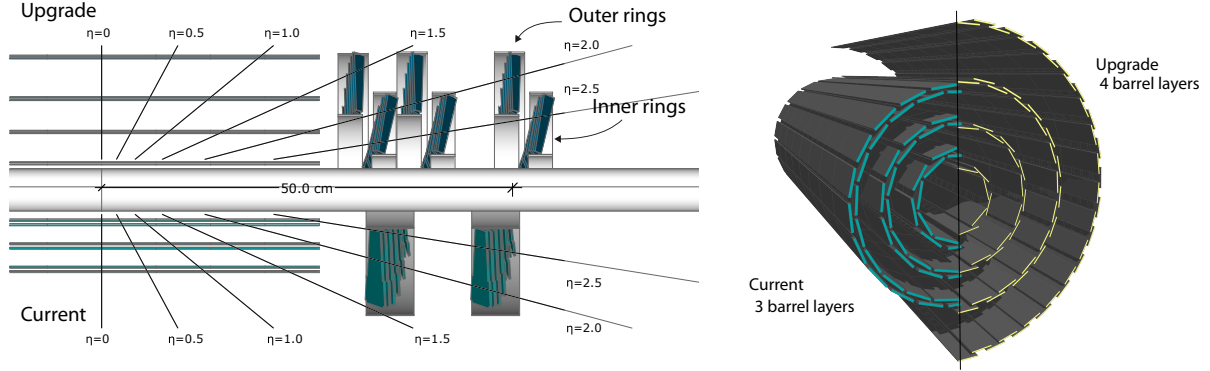


Figure 2: Left: Conceptual layout comparing the different layers and disks in the current and upgrade pixel detectors. Right: Transverse-oblique view comparing the pixel barrel layers in the two detectors.

closer to the interaction point, by 14 mm, at a radius of 30 mm; this will improve the track impact parameter (IP) resolution. The radius of the outermost layer, now the fourth layer, increases to 160 mm, closer to the Tracker Inner Barrel (TIB) layers; this will reduce the rate of fake tracks and mitigate future inefficiencies in the TIB. The new detector will have $\sim 123\text{M}$ pixels, almost twice the present system.

The performance of the proposed upgrades to the pixel detector has been studied with a full GEANT simulation of the CMS detector, using complete descriptions of the detector and beam pipe geometries and materials. Both the present and new detectors have been simulated, including emulation of the ROC signal thresholds and data loss. In these studies, CMS track reconstruction has not been re-optimized for the new detector nor have the track selection and the algorithm used for the b-tagging been tuned to the upgrade conditions. The performance presented for the new pixel detector is therefore likely conservative. Studies have been performed for luminosities of $10^{34} \text{ cm}^{-2} \text{ s}^{-1}$ with 25 ns bunch spacing, used as a reference for the present detector, $2 \times 10^{34} \text{ cm}^{-2} \text{ s}^{-1}$ with a 25 ns bunch spacing (pile-up of 50) and for the extreme case of a 100 pile-up corresponding to a 50 ns bunch spacing at the same luminosity. The performance comparison of the current and new detectors is presented in Fig. 3. It shows the average efficiency and average rate of fake tracks. Major improvements in the track reconstruction efficiency are achieved with the new design, resulting from the increased number of

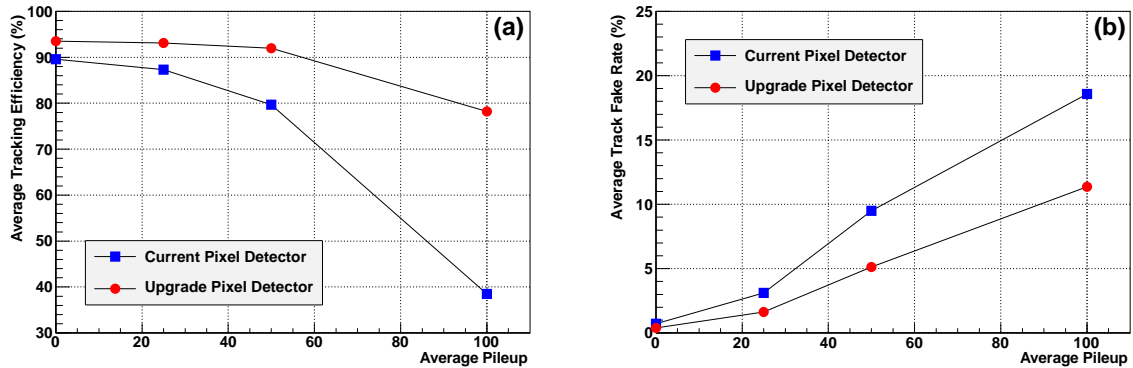


Figure 3: Average tracking efficiencies (a) and fake rates (b) as a function of pile-up for the $t\bar{t}$ event selection.

layers (disks) and the mitigation of the ROC data loss.

Another benefit with the new detector is improved resolution on measurements of the transverse and longitudinal components of the track impact parameter (IP), and of the primary vertex position. These resolutions are key elements in b-tagging efficiency. The improvements result from the increase in the number of space points, the lower radius of the first layer, the lower ROC data loss and signal thresholds and the reduced detector mass. Expected IP resolutions estimated with simulated muon tracks in different pile-up conditions are shown in Fig. 4. The expected primary-vertex resolution is estimated using the $t\bar{t}$ event sample. It is presented in Fig. 5 for different pile-up conditions. The b-tagging performance of the new pixel detector has been studied for the "Combined Secondary Vertex" (CSV) algorithm with the $t\bar{t}$ event sample. The CSV is a multivariate method using both track IPs and secondary vertex reconstruction. Fig. 6 shows the fraction of c jets or light-quark jets (u,d,s) misidentified as b jets as a function of the efficiency to tag the true b jets. Figure 7 shows this efficiency as a function of pile-up for typical mis-tagging fractions.

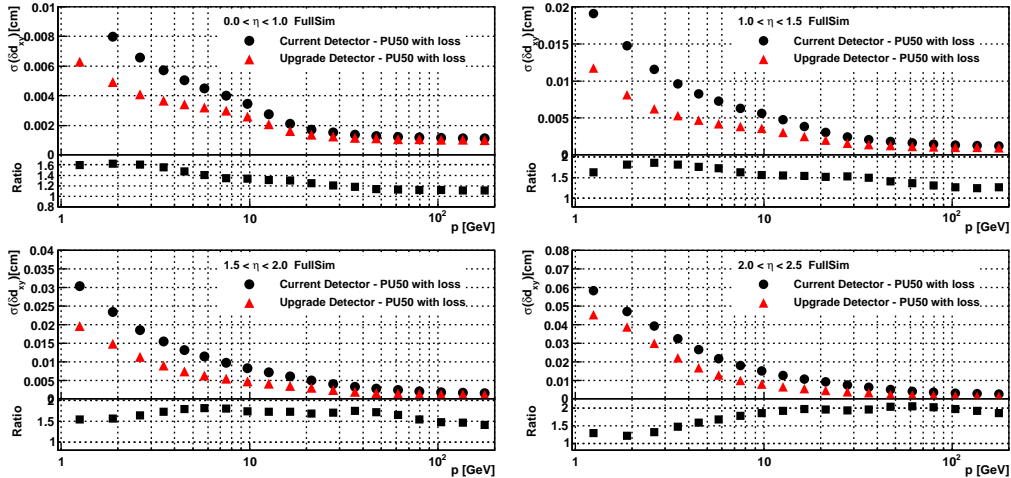


Figure 4: Transverse IP resolution for muon tracks as a function of momentum for different pseudorapidity regions. The current and new detectors are represented with black dots and red triangles, respectively.

The results of these studies indicate that while performance would be seriously compromised without the proposed upgrade, with the new detector there is no degradation, and in several cases significant improvement, to the performance of the reconstruction of the objects that are relevant for physics. These studies give us confidence in the validity (as concerns tracking and b-tag performance) of the extrapolations to 300 fb^{-1} of physics results presented in this report.

3.1.2 Hadron Calorimeter Upgrade

The CMS hadron calorimetry system (HCAL) has four major sections: the HCAL Barrel (HB), HCAL Endcap (HE), HCAL Outer (HO), and HCAL Forward (HF). The HCAL upgrade takes advantage of new technologies that have become available since the design and construction of the original calorimeters and improves the performance of the calorimeters as built, primarily through the replacement of the phototransducers and electronics. It will also address and mitigate weaknesses that have been identified in the current systems.

The upgrades of the HF and HB/HE systems are based on the replacement of the phototransducers for these calorimeters. For the HF, the current single-anode PMTs will be replaced by

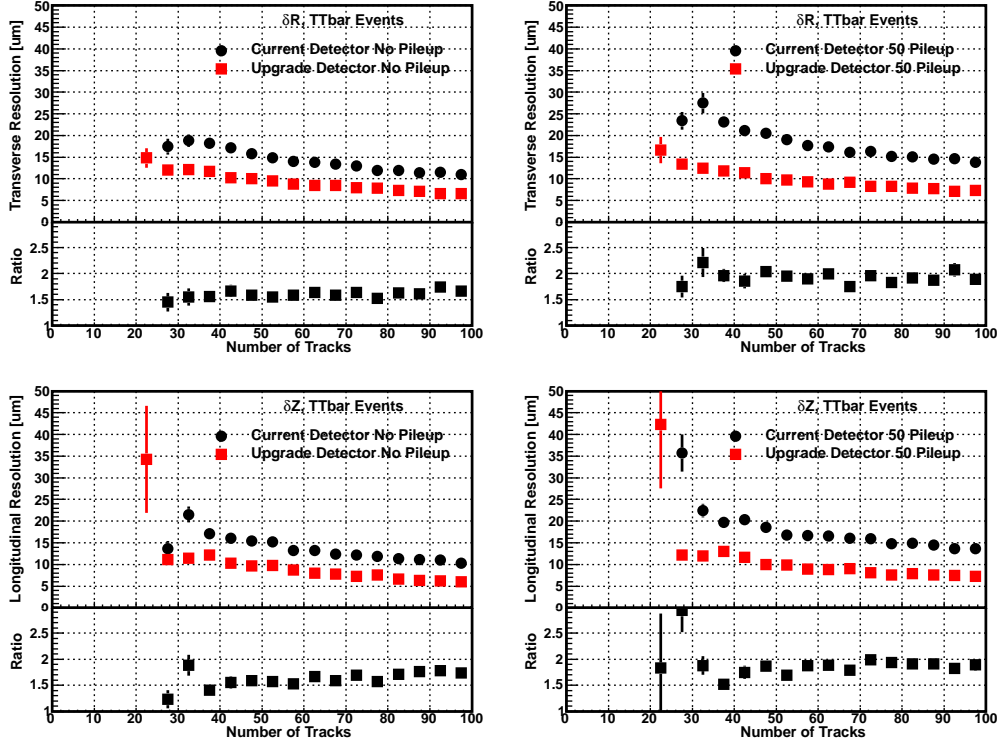


Figure 5: Transverse (top) and longitudinal (bottom) primary vertex position resolutions as a function of the number of tracks; without pile-up (left) and at a 50 pile-up (right). The current and new detectors are respectively represented with black dots and red squares.

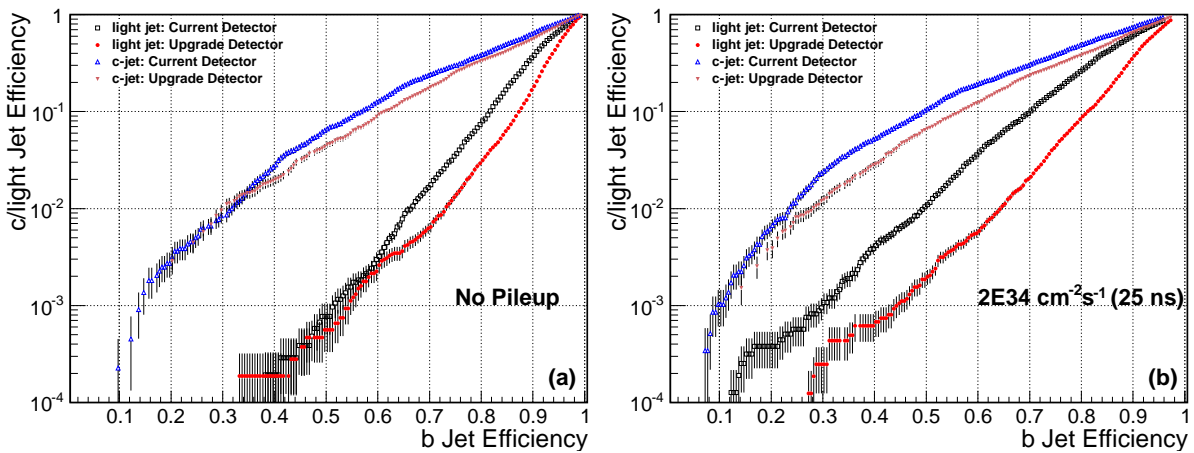


Figure 6: Fraction of c jets or light-quark jets misidentified as b jets for the current (blue/black) and upgraded (red) detectors as a function of the efficiency to tag true b jets in the absence of pile-up (left), and with 50 pile-up (right).

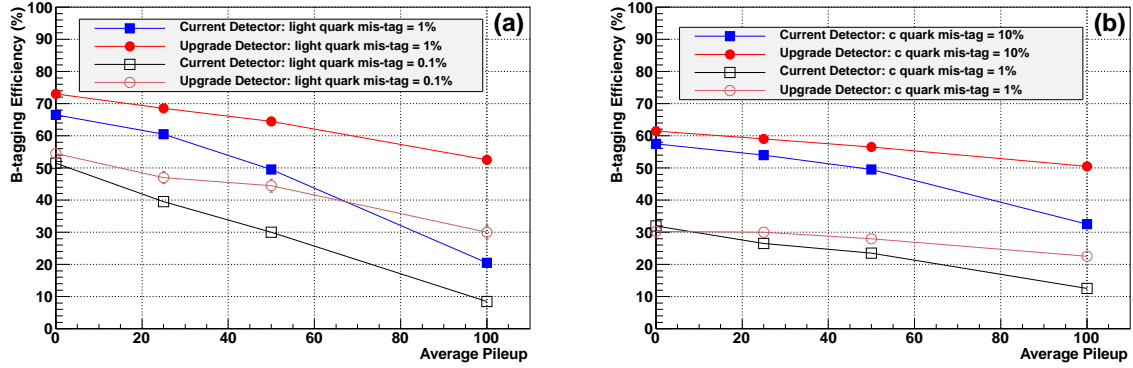


Figure 7: The b-tagging efficiency of the current (blue/black) and upgraded (red) detectors as a function of pile-up for typical values of mistagging fractions for light-quark jets (left) and c jets (right).

multi-anode PMTs with increased quantum efficiency. As discussed below, the upgrade uses dual-anode readout of the PMTs and a new TDC capability to suppress background from spurious signals and recover the calorimeter response where possible. For the HB/HE systems, a newly-proven technology the Silicon Photomultiplier (SiPM) will be used. These new photodetectors will be followed by a common chain of upgraded electronics which provides increased robustness to channel or link failures and a greatly-enhanced capacity for calculating and delivering inputs to the calorimeter trigger. The upgraded electronics should tolerate the full radiation dose anticipated through HL-LHC operation, for 3000 fb^{-1} total luminosity.

The performance gains of the upgraded detector originate from the superior characteristics of the new photodetectors to be installed in the barrel, endcap, and forward calorimeters and from the expanded functionalities of the proposed front-end and back-end electronics upgrades. The SiPM photodetectors with newly designed readout chips provide an order of magnitude higher signal-to-noise ratio in the barrel and endcap calorimeters. In the forward calorimeter the multi-anode signals provide redundant sampling of the light from a single calorimeter cell and high quantum efficiency for measuring Cerenkov signals while the new TDC capability allows rejection of background.

In the HB and HE, the switch to the SiPM with its much-decreased noise level and higher gain allows longitudinal segmentation of the calorimeter without introducing excessive noise. Figure 8 shows the current proposed depth segmentation. This depth segmentation allows better determination of hadronic shower development. Studies in simulation of particle-flow behavior at high pile up show large numbers of anomalous hits and large clusters of energy as the particle flow algorithms can no longer distinguish individual high-energy particle showers. The addition of depth segmentation eliminates the anomalous hits and improves the association of clusters and tracks which is crucial for particle-flow techniques.

Depth segmentation improvements, along with the high photon-detection-efficiency of the SiPMs, will also allow better management of the radiation damage which will occur with the high- η region of the HE calorimeter. The longitudinal segmentation of the hadron calorimeter will also provide shower profile information to be used to verify that electromagnetic particles identified in the ECAL have little energy in the HCAL. In particular, the segmentation suppresses the influence of pileup particles that contribute to the first layer of HCAL but not to deeper layers. Similarly, the deepest segment of HCAL can be useful for efficient identification of prompt muons and rejection of muons produced in the decay of hadrons in flight.

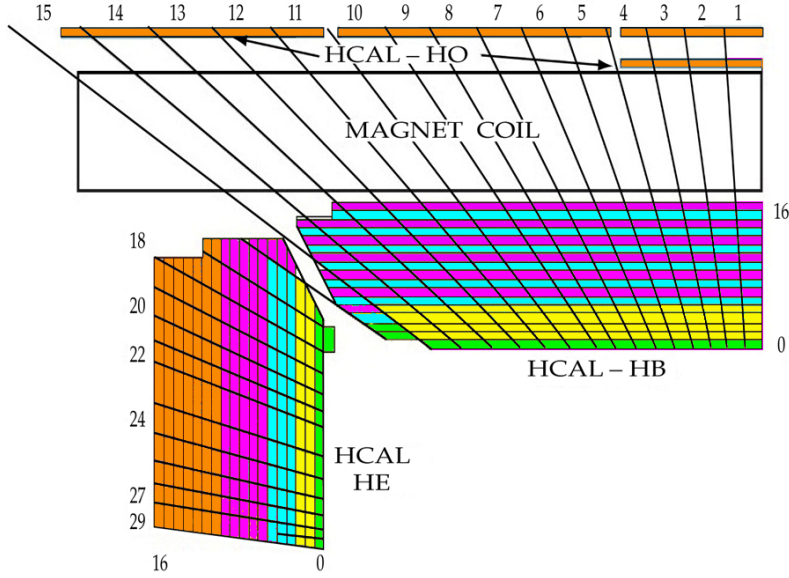


Figure 8: Current proposed depth segmentation structure for the HB and HE calorimeters, made possible by the use of SiPM photodetectors.

3.1.3 L1 Trigger Upgrade

The first level (L1) trigger for the CMS experiment must facilitate a physics program wherein comparable sensitivity to electroweak scale physics and TeV scale searches is maintained with respect to the pre-LS1 program. It must do so with an increased LHC center-of-mass energy near 14 TeV, with pile-up of about 50 interactions per crossing, and with a luminosity in excess of $2 \times 10^{34} \text{ cm}^{-2}\text{s}^{-1}$. With the increase in energy, luminosity and pile-up, a substantial increase in trigger thresholds would be required to fit within the nominal limit of 100 kHz, especially for pile-up sensitive multi-object triggers. This would have a detrimental impact on the physics acceptance of the CMS experiment, in particular at the electroweak scale where the study of the couplings of the newly discovered Higgs boson is a priority. An upgrade to the L1 trigger hardware that expands both the capability and flexibility of the system is needed. The L1 trigger upgrade will provide the following:

- Improved electromagnetic object isolation using calorimeter energy distributions with pile-up subtraction;
- Improved jet finding with pile-up subtraction;
- Improved hadronic tau identification with a smaller fiducial area;
- Improved muon transverse momentum (p_T) resolution in difficult regions;
- Isolation of muons using calorimeter energy distributions with pile-up subtraction;
- Improved global Level-1 trigger menu with a greater number of triggers and with more sophisticated relations involving the input objects.

The L1 trigger upgrade will also be flexible and scalable to accommodate future upgrades to the experiment beyond the present ones such as those required for the HL-LHC physics program. The upgraded system will form a basis to which additional inputs can be easily incorporated and to which additional processing power can be added in a straightforward way.

To meet these requirements, CMS will upgrade the electronics for the calorimeter trigger, the muon trigger, and the global trigger. Additional interconnections between these systems will

also be provided, to implement algorithms such as muon isolation. As noted above, a key feature of this upgrade is that it will offer a large increase in flexibility beyond that provided by the current trigger system. Flexibility has been important in adapting to the rapidly evolving running conditions since LHC start-up, and will continue to be needed in order to implement further rate reduction and efficiency improvements as algorithms improve. This increased flexibility will be accomplished by using high bandwidth optical links for most of the data communication between trigger cards, and by using modern, large FPGAs and large memory resources for the trigger logic. The use of optical links allows the architecture to be readily changed, while large FPGAs allow for algorithms to evolve as needed.

The current L1 makes use of a large number of different electronics cards. CMS plans to use the upgrade as an opportunity to reduce this diversity, basing the upgrade on a small number of general-purpose designs. It is planned to pursue a similar path of consolidation on the software and firmware side of the project, increasing that which is common to all components of the trigger. The electronic systems will be implemented in the telecommunications standard μ TCA, evolving away from the VME framework used previously, to take advantage of additional flexibility and higher bandwidth. The proposed upgrade maintains the overall architecture and functionality of the present trigger system, with upgrades to each of the main areas of calorimeter, muon and global trigger systems. The schedule for the upgrade foresees parallel commissioning during the LHC restart after LS1 in 2015. The upgraded trigger system is planned to be available for CMS data taking in 2016.

To study the performance of the upgraded L1 trigger, we prepared simplified trigger menus for the present CMS and trigger upgrade scenarios. These simplified menus contain a small sample of algorithms that capture much of the important physics processes and account for about 80% of the L1 rate in 2012 operations. These menus are used to illustrate typical L1 trigger thresholds that will be attainable with the upgrade. The thresholds are determined not only by the individual rate for each algorithm but also to the total rate of the full menu, which is required to remain below 100 kHz. For any given event, several trigger criteria may be satisfied. Such overlaps are accounted for when estimating the rate of the full menu. Using fully simulated Monte Carlo samples of signal and background processes, the performance of key analyses in the CMS physics program outlined above was evaluated using the plateau efficiencies of the triggers in these simplified menus. An assessment was done by comparing the analysis efficiencies that result from the use of the current L1 menus with those that result from using the upgraded L1 menus. The studies presented applied the analysis strategies used on the 7/8 TeV pp collision data as closely as possible. The results are summarized in Fig. 9.

3.2 Phase 2 Upgrades to the CMS Experiment

Due to radiation damage, aging, and the challenges of even higher instantaneous luminosities for the HL-LHC, a number of additional major upgrades to the CMS detector will be required in order to preserve the ability to carry out the diverse physics program of the CMS experiment. The performance of the tracking system will significantly degrade with radiation aging, and a new tracker will be needed. The new tracker will have substantially less material and in addition to providing improved tracking capability in a dense charged particle environment, will also provide tracks to the L1 trigger, allowing a substantial increase in trigger functionality. We are also examining a possible upgrade to the front-end electronics and high-level trigger systems, which would allow up to 1 MHz L1 readout and up to 10 kHz event storage rate.

The upgrade must ensure that precision electromagnetic calorimetry and robust jet and missing transverse energy reconstruction capability are maintained at the HL-LHC. Issues are particu-

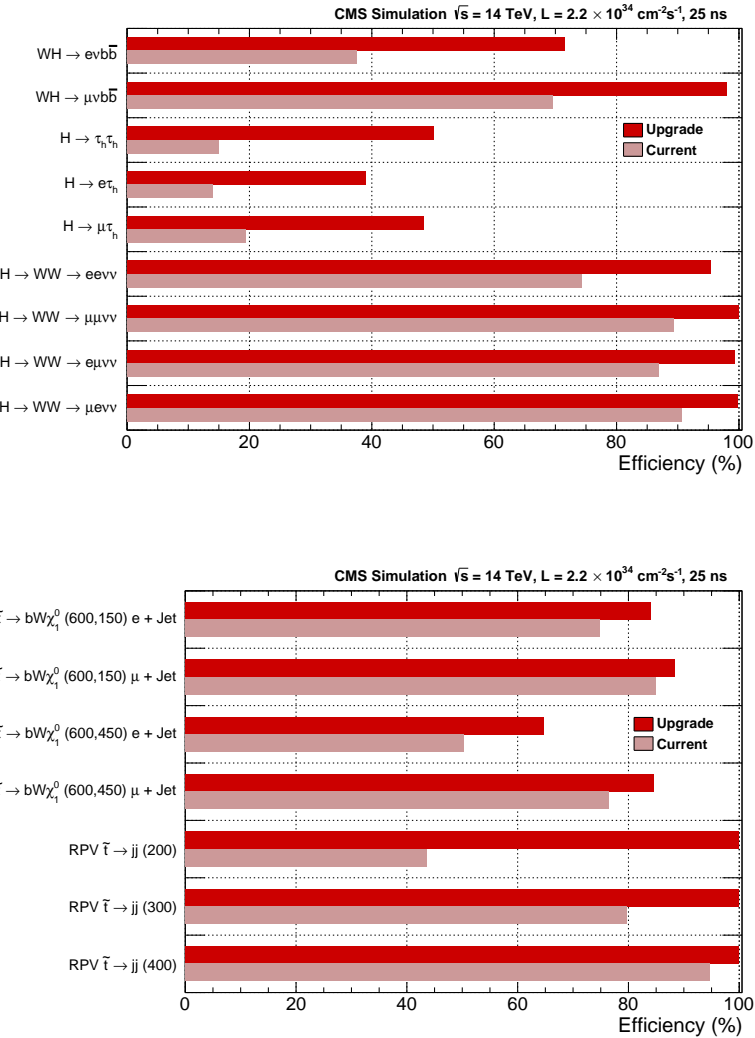


Figure 9: Signal efficiency obtained for the current and an upgraded L1 trigger system at $L = 2 \times 10^{34} \text{ cm}^{-2}\text{s}^{-1}$ for selected Higgs (top) and SUSY (bottom) channels.

larly severe in the endcap region, where the present calorimeters will suffer radiation damage and where event pile-up is more pronounced. This region has critical importance in major parts of the physics program (e.g. vector-boson-fusion Higgs production and vector-boson-scattering studies). Both the electromagnetic and hadronic endcap calorimeters must be replaced. Studies are underway to determine the optimal choice for technology and design. An option is under consideration to extend tracking beyond $\eta = 2.5$ with additional pixel disks to improve particle flow reconstruction and pile-up mitigation in this region. The use of precision timing measurement which could be integrated into an electromagnetic preshower detector is also being investigated. Such a system could provide further pile-up mitigation.

Several Phase 2 upgrade scenarios are under study using both parametrized detector resolutions/responses with which different configurations can be easily compared, and full GEANT simulations for investigations that require more complex treatment. The result of these studies will be included along with a description of the design considerations in a Technical Proposal for the Phase 2 upgrade, anticipated in 2014.

Since the studies to optimize the design choices for Phase 2 are ongoing, it is challenging to ex-

trapolate the performance of physics results with the 3000 fb^{-1} dataset. This complication is in addition to the inherent difficulty of extrapolating to a dataset more than 100 times larger than the current dataset on which the studies are based and whose systematic uncertainties (both experimental and theoretical) will evolve over the next decade. The present CMS expectation of this evolution is discussed in subsequent Sections.

4 Higgs Boson Properties

The year 2012 will be remembered as the year of the Higgs boson discovery [4, 5]. Hypothesized more than 40 years ago, the Higgs boson holds the key to understanding how fundamental particles acquire their mass and how the electroweak symmetry is broken. The observation of a Higgs boson by the ATLAS and CMS experiments at the LHC has opened a new era for particle physics, namely precision consistency tests of the SM Higgs boson.

Five main decays have been studied: $\gamma\gamma$, ZZ , WW , $\tau\tau$, and bb , using data samples corresponding to integrated luminosities of up to 5.1 fb^{-1} at 7 TeV and up to 19.6 fb^{-1} at 8 TeV. The mass of the new boson has been measured from the $\gamma\gamma$ and $ZZ \rightarrow 4\ell$ channels to be $125.7 \pm 0.4 \text{ GeV}$ [14]. The event yields obtained by the different analyses targeting specific decay modes and production mechanisms are within current uncertainties consistent with those expected for the SM Higgs boson. The best-fit signal strength for all channels combined, expressed in units of the SM Higgs boson cross section, is 0.80 ± 0.14 [14]. Additional channels have been studied including decays to two muons and $Z\gamma^*$. The consistency of the couplings with those predicted for the SM Higgs boson is tested in various ways, and no significant deviations have been found. Figure 10 shows the results of a coupling fit assuming no BSM decays. A second fit allowing for BSM decays restricting the effective couplings to vector bosons is used to extract a 95% confidence level upper limit of 52% on the branching fraction for undetected Higgs decays [14]. Direct searches for a standard-model-like Higgs boson produced in association with a Z boson or in vector boson fusion production and decaying to invisible particles yields an observed (expected) 95% confidence level upper limit on the branching fraction of the Higgs boson to invisible particles is 54% (46%) [20, 21]. The limits can be translated in the context of dark matter models, strongly constraining them.

The spin-parity of the boson has been studied, and the pure scalar hypothesis found to be consistent with the observation when compared to six other spin-parity hypotheses. The data disfavor the pure pseudoscalar hypothesis 0^- with a CL_s value of 0.16%, and disfavor the pure spin-2 hypothesis of a narrow resonance with the minimal couplings to the vector bosons with a CL_s value of 1.5%. The spin-1 hypotheses are disfavored with an even higher confidence. The measurement of the fraction of a CP-violating contribution to the decay amplitude expressed through the fraction of the corresponding decay rate is $f_{a3} = 0.00^{+0.23}_{-0.00}$, or equivalently $f_{a3} < 0.58$ at 95% CL [7].

Precise measurements of the new boson's properties are of utmost importance. More data are needed to check whether the properties of this new state imply BSM physics. The key properties are the couplings to each fermion and boson, which are predicted by the standard model. Perhaps the most important measurement after the discovery of the Higgs boson is the measurement of the Higgs potential itself. This can be probed with the study of multiple Higgs boson production. Previous studies have shown that a measurement [22] of multiple Higgs boson production is possible with a dataset of 3000 fb^{-1} at the LHC. Promising final states are those which allow a precision measurement of the mass of one of the two Higgs bosons or have large branching fraction, e.g. the $bb\gamma\gamma$ or $bb\tau\tau$ final states, which allow to reduce the experimental backgrounds. It is interesting to note that multiple Higgs boson production can

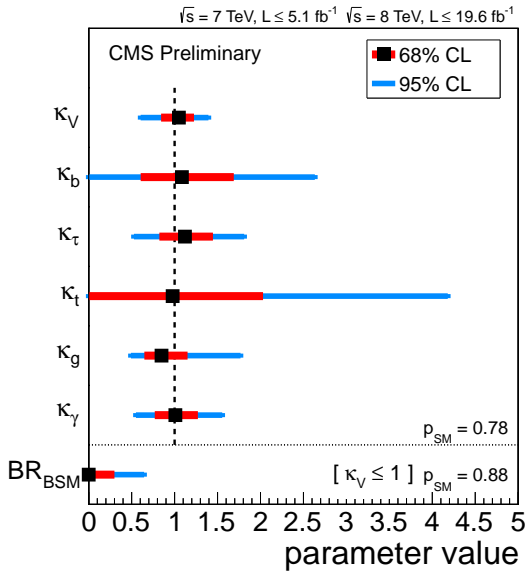


Figure 10: The best fit of the Higgs boson coupling parameters are shown, with the corresponding 68% and 95% CL intervals, and the overall p-value (p_{SM}) of the SM Higgs hypothesis is given. The result of the fit when extending the model to allow for BSM decays, while restricting the effective coupling to vector bosons to not exceed unity ($\kappa_V \leq 1.0$), is also shown.

be increased in BSM scenarios like the MSSM.

4.1 Extrapolation Strategy

In this summary only measurements that have been made public by CMS as measurements applied to the 7 and 8 TeV data are used. The results are extrapolated to larger datasets of 300 and 3000 fb⁻¹ and a center-of-mass energy of 14 TeV by scaling signal and background event yields accordingly. In order to study the precision of future measurements, a number of assumptions are made. As stated in the introduction, the underlying assumption of the extrapolations is that future CMS upgrades will provide the same level of detector and trigger performances achieved with the current detector in the 2012 data taking period. The extrapolations do not take into consideration those channels that were not utilized in the currently available dataset, and there is no attempt to optimize the measurement in order to minimize the uncertainties on Higgs coupling measurements. Extrapolations are presented under two uncertainty scenarios. In Scenario 1, all systematic uncertainties are left unchanged. In Scenario 2, the theoretical uncertainties are scaled by a factor of 1/2, while other systematic uncertainties are scaled by the square root of the integrated luminosity. The comparison of the two uncertainty scenarios indicates a range of possible future measurements. The extrapolation without theoretical uncertainties is also presented, to illustrate the importance of reducing those uncertainties in the future. Systematic uncertainties are inputs to the fits. They can be further constraint by the data when extracting the signal strength, coupling modifier or ratios of such. Similar extrapolations have been discussed in [3].

4.2 Search channels

Higgs cross sections and coupling measurements are obtained by combining information from many Higgs production and decay channels. Table 1 lists the main features of these channels, namely the exclusive final state and the approximate instrumental mass resolution. The simultaneous analysis of the data selected by all individual analyses accounts for all statistical and

systematic uncertainties and their correlations.

Table 1: Summary of the information on the analyses used as input in this combination, including decay mode, production channel (tag), final states, analysis categories, mass resolution, and documentation.

H decay	prod. tag	exclusive final states	cat.	res.	ref.
$\gamma\gamma$	un>tagged	$\gamma\gamma$ (4 diphoton classes)	4	1-2%	
	VBF-tag	$\gamma\gamma + (jj)_{\text{VBF}}$	2	<1.5%	
	VH-tag	$\gamma\gamma + (e, \mu, \text{MET})$	3	<1.5%	[6]
	ttH-tag	$\gamma\gamma$ (lep. and had. top decay)	2	<1.5%	[23]
$ZZ \rightarrow 4\ell$	$N_{\text{jet}} < 2$		3		
	$N_{\text{jet}} \geq 2$	$4e, 4\mu, 2e2\mu$	3	1-2%	[7]
$WW \rightarrow \ell\nu\ell\nu$	0/1-jets	(DF or SF dileptons) \times (0 or 1 jets)	4	20%	[8]
	VBF-tag	$\ell\nu\ell\nu + (jj)_{\text{VBF}}$ (DF or SF dileptons)	2	20%	[24]
	WH-tag	$3\ell 3\nu$ (same-sign SF and otherwise)	2		[25]
$\tau\tau$	0/1-jet	$(e\tau_h, \mu\tau_h, e\mu, \mu\mu) \times$ (low or high p_T^{τ})	16		
	1-jet	$\tau_h\tau_h$	1	15%	
	VBF-tag	$(e\tau_h, \mu\tau_h, e\mu, \mu\mu, \tau_h\tau_h) + (jj)_{\text{VBF}}$	5		
	ZH-tag	$(ee, \mu\mu) \times (\tau_h\tau_h, e\tau_h, \mu\tau_h, e\mu)$	8		[26]
bb	WH-tag	$\tau_h\mu\mu, \tau_h e\mu, e\tau_h\tau_h, \mu\tau_h\tau_h$	4		
	VH-tag	$(vv, ee, \mu\mu, ev, \mu\nu$ with 2 b-jets) \times x	13	10%	[27]
	ttH-tag	$(\ell$ with 4, 5 or ≥ 6 jets) \times (3 or ≥ 4 b-tags); $(\ell$ with 6 jets with 2 b-tags); ($\ell\ell$ with 2 or ≥ 3 b-jets)	6		
			3		[28]
$Z\gamma$	inclusive	$(ee, \mu\mu) \times (\gamma)$	2		[29]
$\mu\mu$	0/1-jets	$\mu\mu$	12		
	VBF-tag	$\mu\mu + (jj)_{\text{VBF}}$	3	1-2%	[30–32]
invisible	ZH-tag	$(ee, \mu\mu) \times (\text{MET})$	2		[21]

4.3 Signal Strength

The signal strength modifier $\mu = \sigma/\sigma_{\text{SM}}$, obtained in the combination of all search channels, provides a first compatibility test. Figure 11 and Table 2 show the μ uncertainties obtained in different sub-combinations of search channels, organized by decay mode for an integrated dataset of 300 fb^{-1} and 3000 fb^{-1} . We predict a precision 6–14% for 300 fb^{-1} and 4–8% for a dataset of 3000 fb^{-1} . Studies show that future measurements of the signal strength will be limited by theoretical uncertainty of the signal cross section, which is included in the fit. Figure 13 (left) shows the uncertainty on the signal strength omitting the uncertainties from QCD scale and PDFs for signal and background.

Table 2: Precision on the measurements of the signal strength per decay mode for a SM-like Higgs boson. These values are obtained at $\sqrt{s} = 14 \text{ TeV}$ using an integrated dataset of 300 and 3000 fb^{-1} . Numbers in brackets are % uncertainties on the measurements estimated under [Scenario2, Scenario1], as described in the text. For the direct search for invisible Higgs decays the 95% CL on the branching fraction is given.

$L (\text{fb}^{-1})$	$\gamma\gamma$	WW	ZZ	bb	$\tau\tau$	$Z\gamma$	$\mu\mu$	inv.
300	[6, 12]	[6, 11]	[7, 11]	[11, 14]	[8, 14]	[62, 62]	[40, 42]	[17, 28]
3000	[4, 8]	[4, 7]	[4, 7]	[5, 7]	[5, 8]	[20, 24]	[20, 24]	[6, 17]

The direct search for invisible Higgs decays in events produced in association with a Z boson yields a 95% confidence level upper limit on the branching fraction of 28 (17)% for Scenario 1 and 17 (6.4)% for Scenario 2 for 300 (3000) fb^{-1} .

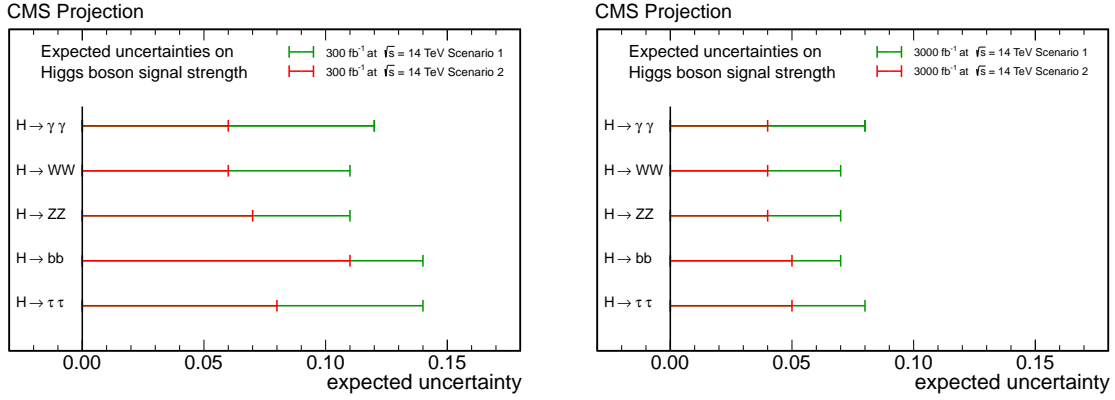


Figure 11: Estimated precision on the measurements of the signal strength for a SM-like Higgs boson. The projections assume $\sqrt{s} = 14$ TeV and an integrated dataset of 300 fb^{-1} (left) and 3000 fb^{-1} (right). The projections are obtained with the two uncertainty scenarios described in the text.

4.4 Coupling-Modifier Fit

The event yield for any (production) \times (decay) mode is related to the production cross section and the partial and total Higgs boson decay widths via the narrow-width approximation:

$$(\sigma \cdot \text{BR}) (x \rightarrow H \rightarrow ff) = \frac{\sigma_x \cdot \Gamma_{ff}}{\Gamma_{\text{tot}}}, \quad (1)$$

where σ_x is the production cross section through the initial state x , Γ_{ff} is the partial decay width into the final state ff , and Γ_{tot} is the total width of the Higgs boson. In particular, σ_{ggH} , Γ_{gg} , and $\Gamma_{\gamma\gamma}$ are generated by quantum loops and are directly sensitive to the presence of new physics. The possibility of Higgs boson decays to BSM particles, with a partial width Γ_{BSM} , is accommodated by keeping Γ_{tot} as a dependent parameter so that $\Gamma_{\text{tot}} = \sum \Gamma_{ii} + \Gamma_{\text{BSM}}$, where the Γ_{ii} stand for the partial width of decay to all SM particles. The partial widths are proportional to the square of the effective Higgs boson couplings to the corresponding particles. To test for possible deviations in the data from the rates expected in the different channels for the SM Higgs boson, factors κ_i corresponding to the coupling modifiers are introduced and fit to the data [33].

Figure 12 and Table 3 show the uncertainties obtained on κ_i for an integrated dataset of 300 fb^{-1} and 3000 fb^{-1} . The expected precision ranges from 5–15% for 300 fb^{-1} and 2–10% for a dataset of 3000 fb^{-1} . The measurements will be limited by systematic uncertainties on the cross section, which is included in the fit for the signal strength. The statistical uncertainties on κ_i are below one percent. As for the results on the signal strength, to illustrate the importance of theoretical uncertainties, a fit was performed without considering theoretical systematics. The results are shown in Fig. 13.

The likelihood scan versus $\text{BR}_{\text{BSM}} = \Gamma_{\text{BSM}} / \Gamma_{\text{tot}}$ yields a 95% CL of the invisible BR of 18 (11) % for Scenario 1 and 14 (7) % for Scenario 2 for 300 (3000) fb^{-1} . This scan assumes that the coupling to the W and Z boson are equal to or smaller than the SM values. Fits for ratios of Higgs boson couplings do not require assumptions on the total width or couplings to the W and Z boson. The results are shown in Figure 14 and Table 4.

The measurement of couplings can be extended to first- and second-generation fermions. Previous studies have shown that the Higgs decay to a pair of muons can be observed in gluon-gluon

fusion and via vector-boson fusion production [30–32]. The dimuon events can be observed as a narrow resonance over a falling background distribution. The shape of the background can be parametrized and fitted together with a signal model. Assuming the current performance of the CMS detector, we confirm these studies and estimate a measurement of the $h\mu\mu$ coupling with a precision of 8%, statistically limited in 3000 fb^{-1} .

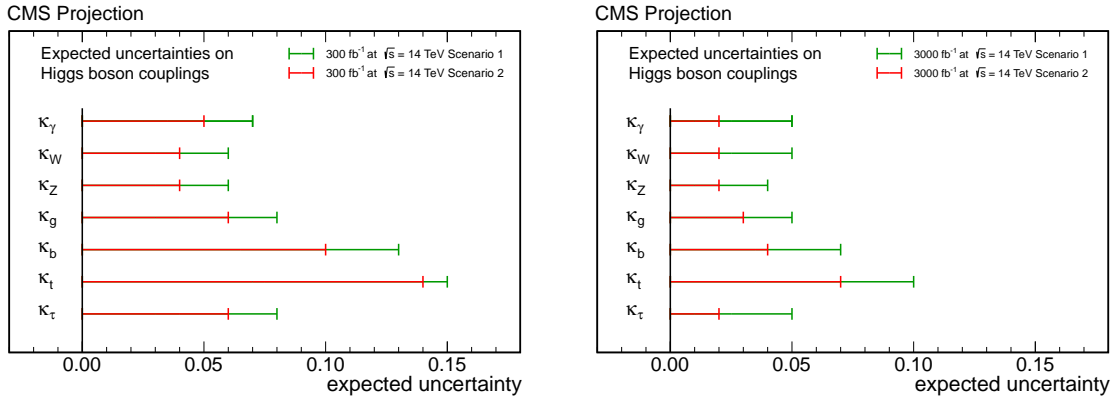


Figure 12: Estimated precision on the measurements of κ_γ , κ_W , κ_Z , κ_g , κ_b , κ_t and κ_τ . The projections assume $\sqrt{s} = 14 \text{ TeV}$ and an integrated dataset of 300 fb^{-1} (left) and 3000 fb^{-1} (right). The projections are obtained with the two uncertainty scenarios described in the text.

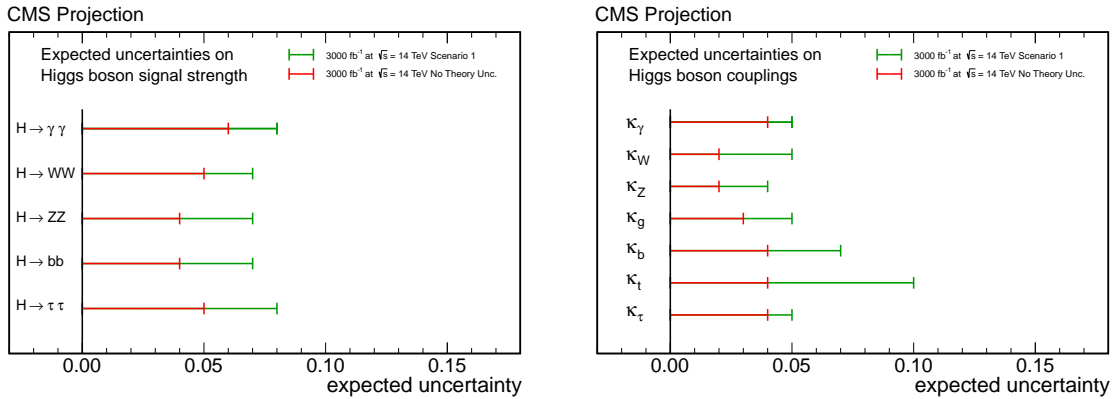


Figure 13: Estimated precision on the signal strengths (left) and coupling modifiers (right). The projections assuming $\sqrt{s} = 14 \text{ TeV}$, an integrated dataset of 3000 fb^{-1} and Scenario 1 are compared with a projection neglecting theoretical uncertainties.

4.5 Spin-parity

Besides testing Higgs couplings, it is important to determine the spin and quantum numbers of the new particle as accurately as possible. The full case study has been presented by CMS with the example of separation of the SM Higgs boson model and the pseudoscalar (0^-) [7]. Studies on the prospects of measuring CP-mixing of the Higgs boson are presented using the $H \rightarrow ZZ^* \rightarrow 4l$ channel. The decay amplitude for a spin-zero boson defined as

$$A(H \rightarrow ZZ) = v^{-1} \left(a_1 m_Z^2 \epsilon_1^* \epsilon_2^* + a_2 f_{\mu\nu}^{*(1)} f^{*(2),\mu\nu} + a_3 f_{\mu\nu}^{*(1)} \tilde{f}^{*(2),\mu\nu} \right). \quad (2)$$

Table 3: Precision on the measurements of κ_γ , κ_W , κ_Z , κ_g , κ_b , κ_t and κ_τ . These values are obtained at $\sqrt{s} = 14$ TeV using an integrated dataset of 300 and 3000 fb^{-1} . Numbers in brackets are % uncertainties on couplings for [Scenario 2, Scenario 1] as described in the text. For the fit including the possibility of Higgs boson decays to BSM particles d the 95% CL on the branching fraction is given.

$L (\text{fb}^{-1})$	κ_γ	κ_W	κ_Z	κ_g	κ_b	κ_t	κ_τ	$\kappa_{Z\gamma}$	$\kappa_{\mu\mu}$	BR_{SM}
300	[5, 7]	[4, 6]	[4, 6]	[6, 8]	[10, 13]	[14, 15]	[6, 8]	[41, 41]	[23, 23]	[14, 18]
3000	[2, 5]	[2, 5]	[2, 4]	[3, 5]	[4, 7]	[7, 10]	[2, 5]	[10, 12]	[8, 8]	[7, 11]

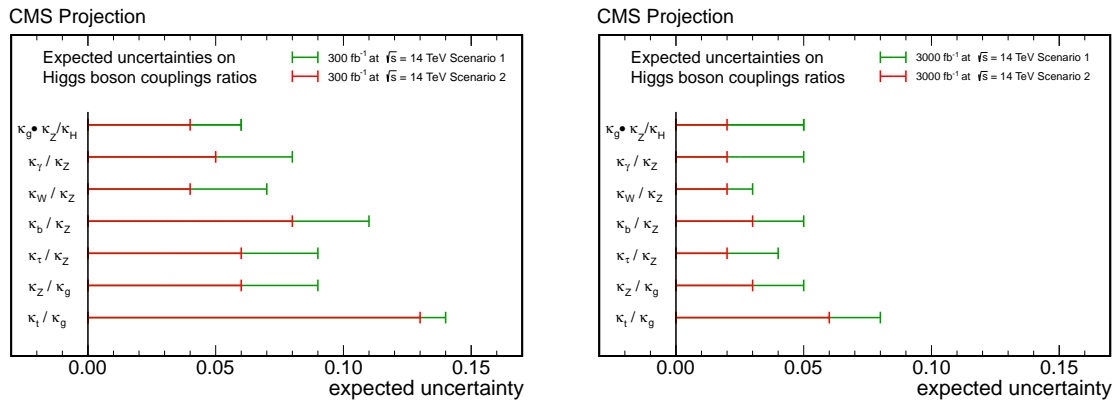


Figure 14: Estimated precision on the measurements of ratios of Higgs boson couplings (plot shows ratio of partial width. It will be replaced by a plot of ratio of couplings by the time of the pre-approval. Uncertainties are 1/2). The projections assume $\sqrt{s} = 14$ TeV and an integrated dataset of 300 fb^{-1} (left) and 3000 fb^{-1} (right). The projections are obtained with the two uncertainty scenarios described in the text.

where $f^{(i),\mu\nu}$ ($\tilde{f}^{(i),\mu\nu}$) is the (conjugate) field strength tensor of a Z boson with polarization vector ϵ_i and v the vacuum expectation value of the Higgs field. The spin-zero models 0^+ and 0^- correspond to the terms with a_1 and a_3 , respectively.

Four independent real numbers describe the process in Eq. (2), provided that the overall rate is treated separately and one overall complex phase is not measurable. For a vector-boson coupling, the four independent parameters can be represented by two fractions of the corresponding cross-sections (f_{a2} and f_{a3}) and two phases (ϕ_{a2} and ϕ_{a3}). In particular, the fraction of CP -odd contribution is defined under the assumption $a_2 = 0$ as

$$f_{a3} = \frac{|a_3|^2 \sigma_3}{|a_1|^2 \sigma_1 + |a_3|^2 \sigma_3},$$

where σ_i is the effective cross section of the process corresponding to $a_i = 1, a_{j \neq i} = 0$. Given the measured value of f_{a3} , the coupling constants can be extracted in any parameterization. For example, following Eq. (2) the couplings will be

$$\frac{|a_3|}{|a_1|} = \sqrt{\frac{f_{a3}}{(1 - f_{a3})}} \times \sqrt{\frac{\sigma_1}{\sigma_3}},$$

where $\sigma_1/\sigma_3 = 6.240$ for a Higgs boson with a mass of 126 GeV.

A fit is performed on the parameter f_{a3} , which is effectively a fraction of events (corrected for reconstruction efficiency) corresponding to the 0^- contribution in the $(D_{0^-}, D_{\text{bkg}})$ distribution.

Table 4: Estimated precision on the measurements of ratios of Higgs boson couplings (plot shows ratio of partial width. It will be replaced by a plot of ratio of couplings by the time of the pre-approval. Uncertainties are 1/2). These values are obtained at $\sqrt{s} = 14$ TeV using an integrated dataset of 300 and 3000 fb^{-1} . Numbers in brackets are % uncertainties on the measurements estimated under [scenario2, scenario1], as described in the text.

$L (\text{fb}^{-1})$	$\kappa_g \cdot \kappa_Z / \kappa_H$	κ_γ / κ_Z	κ_W / κ_Z	κ_b / κ_Z	κ_τ / κ_Z	κ_Z / κ_g	κ_t / κ_g	κ_μ / κ_Z	$\kappa_{Z\gamma} / \kappa_Z$
300	[4,6]	[5,8]	[4,7]	[8,11]	[6,9]	[6,9]	[13,14]	[22,23]	[40,42]
3000	[2,5]	[2,5]	[2,3]	[3,5]	[2,4]	[3,5]	[6,8]	[7,8]	[12,12]

Projections of the expected $-2 \ln \mathcal{L}$ values from the fits assuming 300 fb^{-1} and 3000 fb^{-1} are shown in Fig. 15. A 68% (95%) CL limit on the contribution of f_{a3} can be achieved at the level of 0.07 (0.13) with 300 fb^{-1} and 0.02 (0.04) with 3000 fb^{-1} . The analysis is limited by statistical uncertainties up to a high luminosity, but all sources of systematic uncertainties are preserved in the projections.

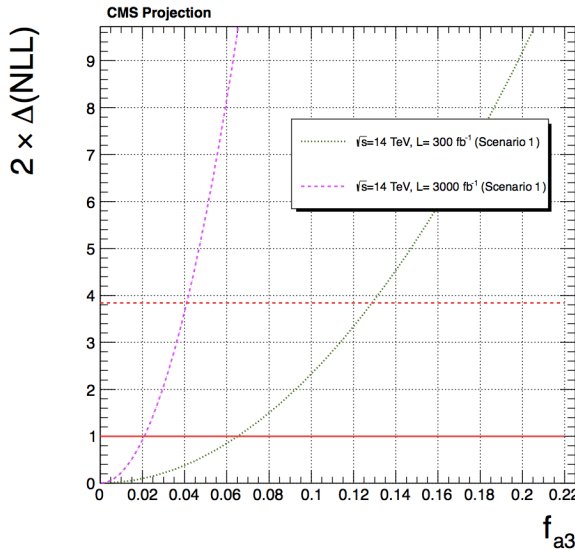


Figure 15: Distribution of expected $-2 \ln \mathcal{L}$ for f_{a3} for the projection to 300 fb^{-1} (green, dotted) and 3000 fb^{-1} (magenta, dot-dashed).

5 Discovery Potential: Supersymmetry

After the observation of a Higgs boson at the LHC, the question about the large quantum corrections to its mass are more pressing than ever. A natural solution to this hierarchy problem would be the cancellation of these corrections from new particles predicted by supersymmetry (SUSY), which have the same quantum numbers as their SM partners apart from spin. No evidence for supersymmetric particles has been found with the data taken at the LHC with $\sqrt{s} = 8$ TeV, but the energy upgrade to 14 TeV together with higher luminosities will open the possibility to access a new interesting mass window in the next years.

Extrapolations of several searches for SUSY by CMS [34–39] are performed by scaling the luminosity and taking into account the change of cross section with higher energy accordingly. The projections are made based on 8 TeV Monte Carlo samples and without optimizing the selections for searches at higher energies and higher luminosities. In “Scenario A” the signal

and background yields, and the uncertainty on the background, are scaled by the ratio of the luminosities (20 fb^{-1} for 8 TeV and 300 fb^{-1} for 14 TeV) and by the ratio of the cross sections for signal and background (σ_{sig} and σ_{bkg}):

$$R_{\text{sig(bkg)}} = \frac{300 \text{ fb}^{-1}}{20 \text{ fb}^{-1}} \times \frac{\sigma_{\text{sig(bkg)}}(14 \text{ TeV})}{\sigma_{\text{sig(bkg)}}(8 \text{ TeV})}. \quad (3)$$

For some analyses, a less conservative scenario, called “Scenario B,” is defined where the relative uncertainty on the background is reduced. These are similar to the Scenarios 1 and 2 used in the Higgs projections discussed in Sec. 4, but not the same in detail and have different implications for SUSY searches where higher mass regions will be progressively searched in the future. The exact procedures differ slightly in projections for different SUSY models and are described in detail in the following sections.

The following models, assuming 100% branching fractions, are considered: gluino-pair production with each gluino decaying to the lightest SUSY particle (LSP) and either a $t\bar{t}$ or $b\bar{b}$ pair; direct stop production with each stop decaying to a top quark and LSP; chargino-neutralino production with final states containing W and Z bosons and missing transverse energy; and direct sbottom production with decay to chargino and top quark. The cross sections for these SUSY particle production processes, computed at the next-to-leading-order accuracy in α_s using Prospino2 [40–42], are shown in Fig. 16.

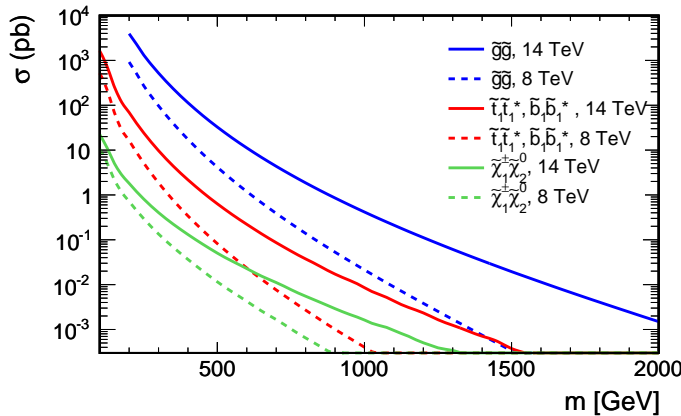


Figure 16: Next-to-leading order cross sections for gluino-pair production, stop-pair (sbottom-sbottom) production, and chargino-neutralino production versus the mass of the pair-produced SUSY particles. The chargino-neutralino production cross section is presented for common $m_{\chi_1^\pm} = m_{\chi_2^0}$ masses.

5.1 Gluino-Pair Production with Four Top Quarks in the Final State

Naturalness predicts not only light third-generation masses, but also gluinos that are not much heavier than a TeV. In this case they could decay to third-generation squarks. This section focuses on gluino-pair production, where each gluino decays to a top and a stop quark that then decays to a top quark and the LSP. This is described by a simplified model, where pair-produced gluinos each decay to a $t\bar{t}$ pair and the LSP (see Fig. 17a). Due to the presence of four W bosons in the final state, a search in the single lepton final state has a large branching fraction ($\sim 40\%$) and good sensitivity. Hence, the sensitivity to this simplified model topology is projected to 14 TeV based on the results obtained in the SUSY search in the single-lepton

channel [34], performed in pp collisions at a center-of-mass energy of $\sqrt{s} = 8 \text{ TeV}$ and corresponding to an integrated luminosity of 19.4 fb^{-1} .

The numbers of signal and background events are scaled from the 8 TeV analysis based on Eq. (3). As the background is dominated by $t\bar{t}$ production, it is scaled up based on the $t\bar{t}$ cross section ratio between 14 TeV and 8 TeV, which is about a factor of 3.9. For Scenario A, the same relative systematic uncertainties as for the 8 TeV analysis are kept, which is a conservative assumption. Nevertheless, the dominant uncertainty of the analysis is the statistical uncertainty from the control regions used for the background estimation, which is reduced by $1/\sqrt{R_{\text{bkg}}}$. Thus, even a more aggressive treatment of the systematic uncertainties would not lead to a sizable improvement on the sensitivity.

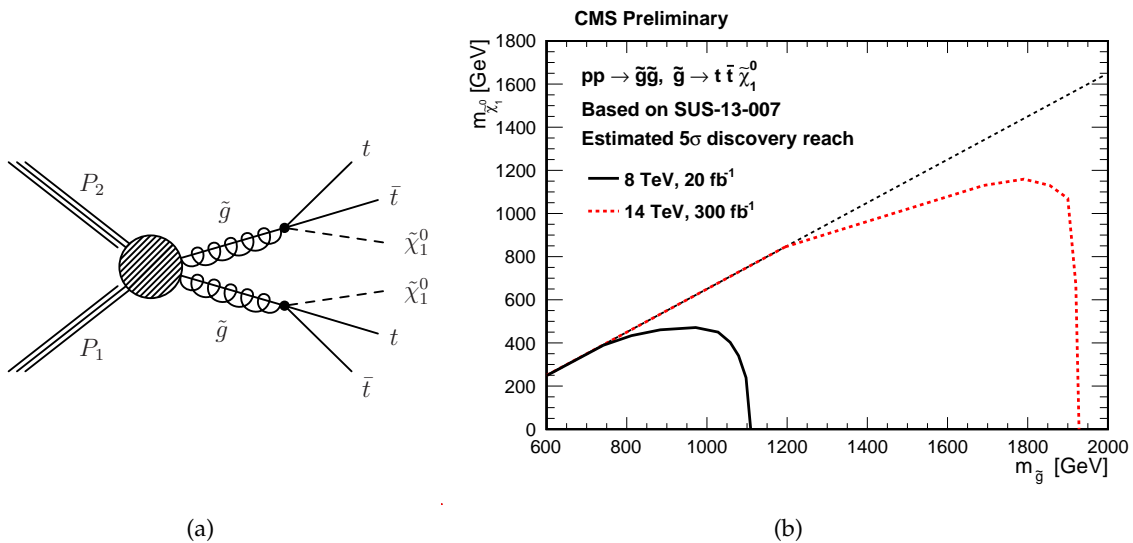


Figure 17: (a) The simplified model topology for gluino production, where the gluinos decay to two top quarks and an LSP each, and (b) the projected 5σ discovery reaches for this model.

The expected significance is calculated using the profile likelihood method and the signal Monte Carlo samples generated with PYTHIA 6 [43] with a CMS custom underlying event tuning [44]. Figure 17b shows the 5σ significance line in the 2-dimensional plane of neutralino versus gluino mass for the different scenarios investigated. Gluino masses up to $\sim 1.9 \text{ TeV}$ for neutralino masses around 0.9 TeV or less can be discovered at 14 TeV with an integrated luminosity of 300 fb^{-1} . It should be noted that the current results are obtained without performing any optimization on the current analysis [34], and further improvements in the sensitivities are expected by re-optimizing the analysis selection for the different scenarios.

5.2 Gluino-Pair Production with Four Bottom Quarks in the Final State

Similar to the gluino decay to four top quarks and two LSPs in the previous section, one can also investigate a model for gluino-pair production, where each gluino decays to $b\bar{b}$ and the LSP (see Fig. 18a). The projection of the sensitivity for 14 TeV is studied based on the results of the search in events with multiple jets, large missing transverse energy, and b tags [35].

The signal and background yields are scaled based on the cross section ratios for the different center-of-mass energies, and the luminosity increase. The systematic uncertainty is conservatively kept the same as for the 8 TeV analysis, corresponding to the Scenario A described above. The signal samples produced with PYTHIA 6 [43] are used for this projection. Figure 18b shows

the projected 5σ discovery reaches for this model. This analysis is sensitive to the discovery of gluinos with masses up to 1.9 TeV for LSP masses of 1.2 TeV or below.

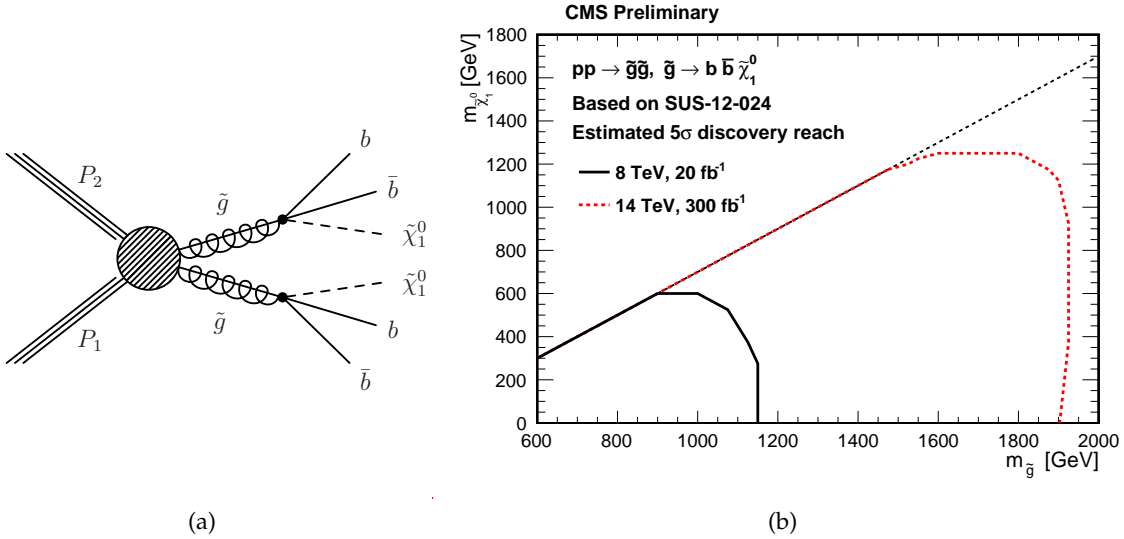


Figure 18: The simplified model topology for gluino production, where the gluinos decay to two bottom quarks and an LSP each (a), and the projected 5σ discovery reaches for this model (b).

For a center-of-mass energy of 14 TeV and an integrated luminosity of 300 fb^{-1} , we expect more than 100 background events in the highest sensitivity bin of the analysis. An actual analysis would be designed in a way that the background is kept smaller, enhancing the sensitivity to a possible signal. Therefore, the given limit can be considered as conservative.

5.3 Stop-Pair Production

One of the most pressing questions for the next run of the LHC is whether third-generation squarks can be observed. Light stop quarks, with masses less than $\sim 1 \text{ TeV}$, are required to cancel the large radiative corrections to the Higgs mass from the top quark without large fine-tuning. One possible production mechanism is the decay of (light) gluinos to stops and sbottoms, if they are lighter than the gluinos and the gluinos are within the LHC reach with 13–14 TeV. These models are studied in the previous Secs. 5.1–5.2. Here, we study the model where the stops are the lightest squarks and are directly produced in pairs. The extrapolation is based on the result obtained from a search in final states with a muon or electron [36]. This analysis has a discovery reach for stop masses of 300–500 GeV and a maximum neutralino mass of 75 GeV for a center-of-mass energy of 8 TeV and an integrated luminosity of 20 fb^{-1} .

The projections to higher energy and luminosity are based on the 8 TeV Monte Carlo simulated samples produced with the MADGRAPH 5 [45] simulation program. For Scenario A, the signal and background yields, as well as the uncertainty on the background, are scaled by the ratios R_{sig} and R_{bkg} , respectively (Eq. (3)). The cross sections for direct stop production are enhanced for 14 TeV by a factor of $\sim 4\text{--}20$ for stop masses of 200–1000 GeV. The main background consists of $t\bar{t}$ events, which are scaled by the cross section ratio. The ratio of the cross sections for the second highest background, $W+\text{jets}$, is smaller than $t\bar{t}$, leading to a conservative background estimation. The signal extrapolation is done in the same way for the less conservative Scenario B, but the uncertainty on the background is reduced by $1/\sqrt{R_{\text{bkg}}}$, as it is assumed that the uncertainty is largely driven by the statistical precision from the control samples, which will

improve with more data. Nevertheless, a fixed lower limit on the relative uncertainty of at least 10% is kept.

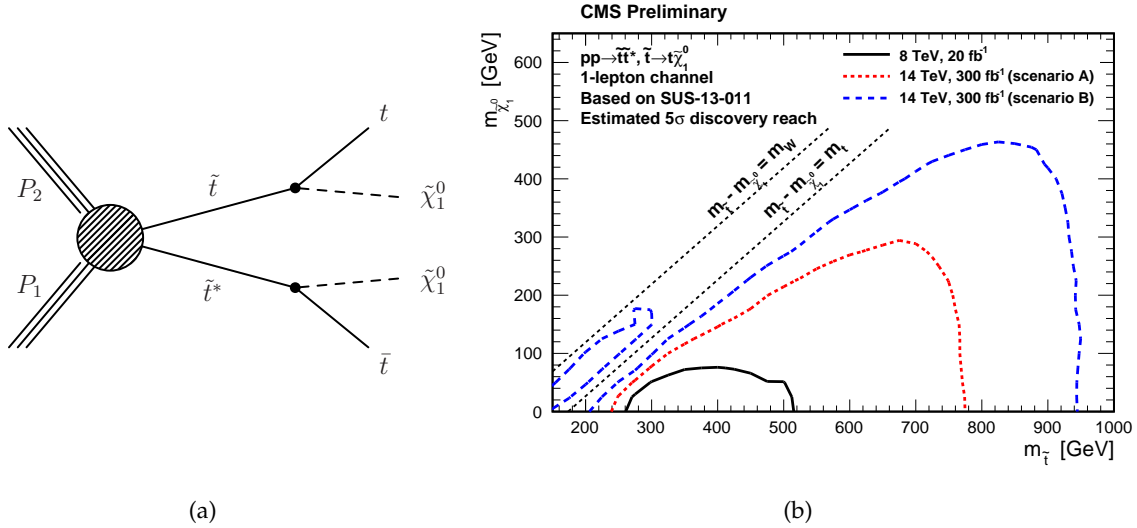


Figure 19: The simplified model topology direct stop production, where the stops decay to a top quark and an LSP each (a), and the projected 5σ discovery reaches for this model (b).

The results are summarized in Fig. 19. A discovery reach for stop masses of 750–950 GeV, and LSP masses of 300–450 GeV, is expected. More stringent selection requirements could suppress the background further, leading to an improvement of the signal-to-background ratio and discovery potential. Also, when searching for stop signals at higher masses, many top quarks from stop decays are highly boosted, but the use of the boosted top taggers are not yet explored to gain extra sensitivity.

5.4 Sbottom-Pair Production with Four W Bosons and Two Bottom Quarks in the Final State

Here, a model is considered where sbottom quarks are relatively light and are directly produced in pairs. The corresponding simplified model assumes that a sbottom quark decays solely to a top quark and a chargino, with the chargino subsequently decaying to a W and the LSP. The model considered here additionally assumes mass splittings such that the top and W are on-shell. The extrapolation is based on the result obtained from a search in a final state with a same-sign lepton pair, jets, b-tagged jets, and missing transverse energy [37].

The background is considered to be composed of two components — one from rare SM processes producing genuine same-sign lepton pairs and another consisting of processes where at least one lepton comes from a jet, hereafter referred to as a fake isolated lepton. These two components comprise over 95% of the background to searches for strongly produced new physics in the same-sign dilepton final state, with rare SM processes contributing 50–80% depending on the search region. The rare SM background consists mainly of processes producing multiple weak bosons or top quarks in the final state, with the largest contribution coming from the production of a $t\bar{t}$ pair in association with a W boson. The background containing fake isolated leptons arises mostly from $t\bar{t}$ events, where one prompt lepton originates from a W boson and the other lepton comes from the decay of a b quark.

We scale the number of signal events N_{sig} by the ratio R_{sig} as defined in Eq. (3). The signal is simulated with MADGRAPH. The signal cross section increases from 8 to 14 TeV approximately by a factor of 5 to 12 for sbottom masses between 300 and 700 GeV. The fake background yield N_{fake} and the rare SM background yield N_{rare} are also scaled by Eq. (3). The scaling of N_{fake} is based on the $t\bar{t}$ cross section ratio, and the scaling of N_{rare} is based on the $t\bar{t}W$ cross section ratio of 3.3 between 14 and 8 TeV [46].

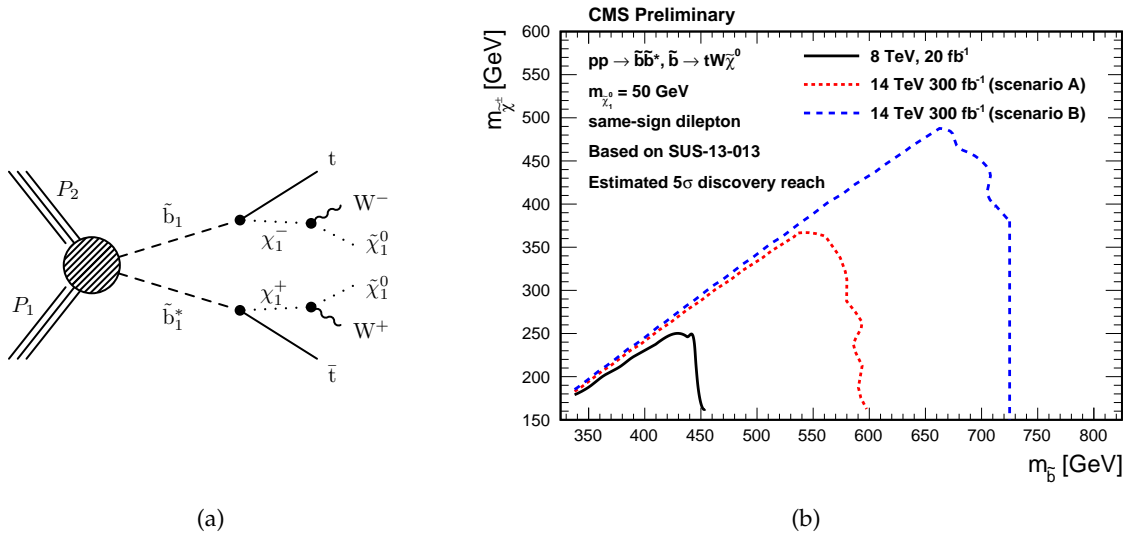


Figure 20: The simplified model topology for direct sbottom production, where the sbottoms decay to a top quark and a chargino each, and the chargino decays to a W boson and a LSP (a), and the projected 5σ discovery reaches for this model (b).

The uncertainty on each component of the background, σ_{rare} and σ_{fake} , is comprised of a 50% systematic uncertainty and a statistical component. For Scenario A, the uncertainties remain the same as for the 8 TeV analysis, except for the statistical uncertainty on the fake prediction, which is scaled down by the square-root of the luminosity and cross section increase, as this uncertainty is driven purely by the fakeable object count in the isolation sideband. For Scenario B, the signal extrapolation is done in the same way, but the systematic uncertainty on the rare SM background is reduced from 50% to 30%, as it can be assumed that the cross sections and kinematic properties of these processes will be measured and better understood. The systematic uncertainty on the fake background is reduced from 50% to 40%.

Figure 20 shows the topology of the investigated simplified model and the 5σ discovery region, which is extended up to sbottom masses of 600–700 GeV and LSP masses up to 350 GeV.

5.5 Chargino-Neutralino Production with Decays to a Z Boson

With higher luminosities, the searches for the electroweak SUSY particles may become increasingly more important. Charginos and neutralinos can be produced in cascade decays of gluinos and squarks or directly via electroweak interactions, and, in the case of heavy gluinos and squarks, gauginos would be produced dominantly via electroweak interactions. Depending on the mass spectrum, the charginos and neutralinos can have significant decay branching fractions to leptons or on-shell vector bosons, yielding multilepton final states. Here the projections of the discovery reach for direct production of $\tilde{\chi}_1^\pm$ and $\tilde{\chi}_2^0$, which decay via W and Z bosons into the LSP ($\tilde{\chi}_1^0$) [39], are presented. This production becomes dominant if sleptons are

too massive and $\tilde{\chi}_1^\pm$ and $\tilde{\chi}_2^0$ are wino-like, which suppresses neutralino-pair production relative to neutralino-chargino production.

The analysis is based on a three-lepton search, with electrons, muons, and at most one hadronically decaying τ lepton. In order to get an estimate for the sensitivity at 14 TeV two different Scenarios (A and B) are considered, as discussed earlier. The results are shown in Fig. 21. The chargino mass sensitivity can be increased to 500–600 GeV, while discovery potential for neutralinos ranges from 150 to almost 300 GeV.

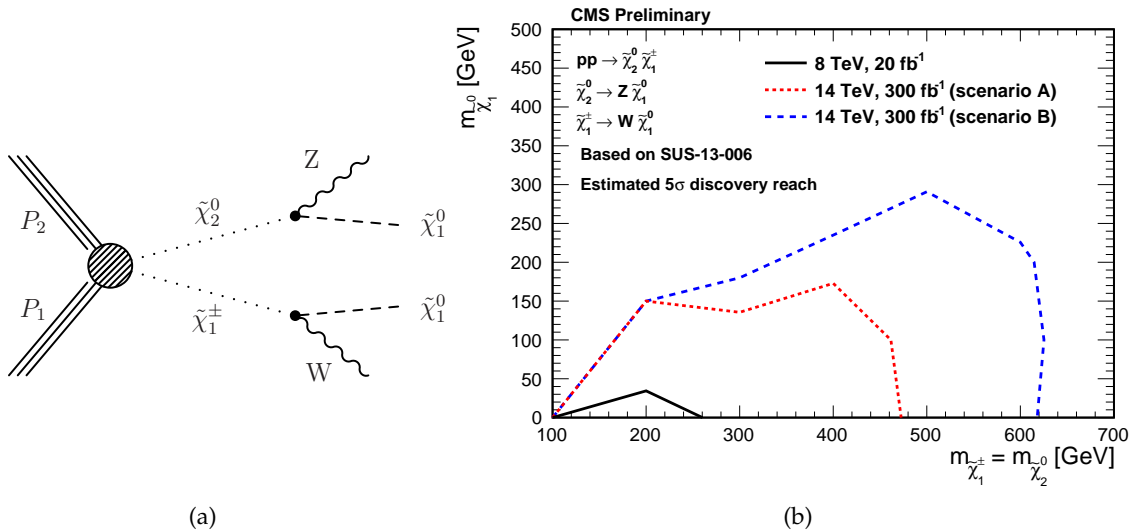


Figure 21: The simplified model topology for direct $\tilde{\chi}_1^\pm \tilde{\chi}_2^0$ production decaying to the $WZ + E_T^{\text{miss}}$ final state (a), and the projected 5σ discovery projections for this model (b).

5.6 Chargino-Neutralino Production with Decays to a Higgs Boson

In this section we also consider chargino-neutralino pair production with a signature that is similar to the one considered in Sec. 5.5, except that here the $\tilde{\chi}_2^0$ instead decays to a Higgs boson and the $\tilde{\chi}_1^0$ LSP. Hence we target the process $\tilde{\chi}_1^\pm \tilde{\chi}_2^0 \rightarrow (W^\pm \tilde{\chi}_1^0)(H\tilde{\chi}_1^0)$ as indicated in Fig. 22(a), and extrapolate the discovery reach based on the analysis of Ref. [47].

The projections are based on the analysis in the single lepton final state, which targets the process $\tilde{\chi}_1^\pm \tilde{\chi}_2^0 \rightarrow (W^\pm \tilde{\chi}_1^0)(H\tilde{\chi}_1^0) \rightarrow \ell\nu b\bar{b} + E_T^{\text{miss}}$. The dominant background in this search is from $t\bar{t}$ production; W bosons produced in association with b-quarks are also relevant. SM backgrounds are suppressed with requirements on E_T^{miss} and related quantities, and we search for a peak in the $m_{b\bar{b}}$ mass distribution consistent with $m_H = 126$ GeV. For the projections, in the conservative scenario we assume $\sigma_{\text{syst}} = 25\%$ as in the current analysis, while in the optimistic scenario we assume a reduction in the systematic uncertainty by a factor of 2.

The estimated 14 TeV discovery reach is shown in Fig. 22. Sensitivity to charginos and neutralinos with masses up to 400–500 GeV is achieved, for LSP masses up to 60–150 GeV. Note that realistic models contain a mixture of the decays $\tilde{\chi}_2^0 \rightarrow Z\tilde{\chi}_1^0$ and $\tilde{\chi}_2^0 \rightarrow H\tilde{\chi}_1^0$, so the sensitivity lies between the projections in this section and those in Sec. 5.5.

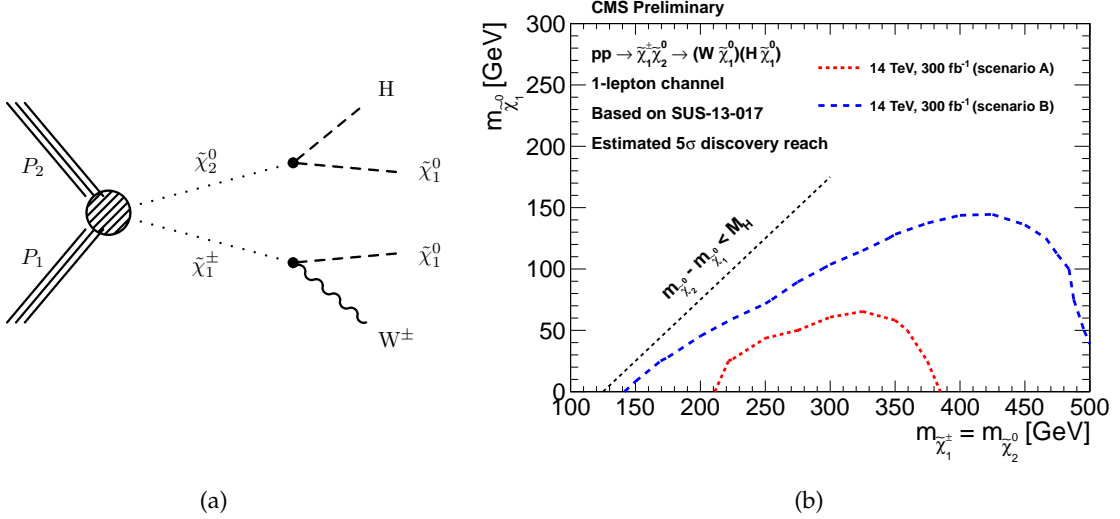


Figure 22: The simplified model topology for direct $\tilde{\chi}_1^\pm \tilde{\chi}_2^0$ production decaying to the $WH + E_T^{\text{miss}}$ final state (a), and the projected 5σ discovery projections for this model (b).

6 Discovery Potential: Exotic New Particles

In this section the discovery potential for exotic signs of new physics with the 14 TeV HL-LHC dataset at CMS is explored. The benchmark channels presented below include searches for additional gauge bosons (Z' and W'), dark matter in the monolepton + MET channel, heavy stable charged particles, and vector-like top partners.

6.1 Searches for Heavy Gauge Bosons Decaying to Lepton Pairs

A search for additional heavy gauge bosons decaying to lepton pairs has been performed with the existing 7 and 8 TeV datasets [48]. In order to project the discovery potential of this search to the HL-LHC scenarios, the background and signal yields are predicted using generator level simulation parameterized by the efficiencies and resolutions measured in the 8 TeV data. The POWHEG event generator and CT10 PDF sets were used to generate $t\bar{t}$ and the dominant Drell-Yan backgrounds, while WW events were generated using PYTHIA. Samples of Z' events were also generated using PYTHIA and no interference effects were considered.

The same acceptance is assumed as in the 8 TeV search. In the electron channel, each electron is required to have $E_T > 35$ GeV and be reconstructed with $|\eta| < 1.442$ (ECAL barrel region) or $1.56 < |\eta| < 2.5$ (ECAL endcap region). At least one electron must be found in the barrel region. Also studied is a case of reduced acceptance due to the degradation of the ECAL endcaps at high luminosity, where both electrons are required to be in the barrel region. In the muon channel, both muons are required to have $p_T > 45$ GeV; one muon must be within $|\eta| < 2.1$ and the other within $|\eta| < 2.4$. The effects of lepton isolation are simulated by requiring $\Delta R > 0.8$ between the leptons and jets in $t\bar{t}$ background events.

Signal and background events are simulated at generator level and smeared to simulate the detector response. The electron identification efficiency is taken to be 88% per electron, from the 8 TeV analysis. The p_T of electrons within the ECAL barrel (endcap) acceptance is smeared by 0.8% (1.6%). Very high energy deposits in a single ECAL crystal (above ~ 1.7 TeV in the barrel and above ~ 3.0 TeV in the endcap) will result in saturation of electronics readout. While

negligible at 8 TeV, this effect will occur more frequently at 14 TeV and is hence included in these projections. The probability for an electron to saturate is predicted using the fraction of electron energy deposited in the leading crystal in fully simulated 8 TeV electron events. Saturating electrons have their energy smeared by 7%, which is the expected resolution from [49]. The muon identification efficiency is 85%, taken from the 8 TeV analysis. The di-muon mass is smeared according to a parameterization of the 8 TeV di-muon mass resolution, which is approximately 10% at 3 TeV. Charge misassignment is not included. The effect of pile-up is observed to be negligible for high energy electrons and muons.

The dominant background for both channels is the Drell-Yan production of lepton pairs. The background due to $t\bar{t}$ is found to self-veto above ~ 1 TeV, where the boost of the top causes the lepton to fail isolation criteria due to the proximity of a b-jet. The background due to WW is expected to be the dominant non-DY background above 1 TeV, but is found to be small (1-2% of the DY). The photon-induced irreducible dilepton background was estimated using the FEWZ3 program [50] and found to be around 5% of the Drell-Yan background in the TeV range relevant for this study, having a negligible impact on the Z' limits. The background due to jets in the electron channel is small and difficult to measure at 8 TeV and is not included in the study.

In order to derive the discovery cross section sensitivity, an empirical fit to both background and signal acceptance is performed as a function of the dilepton mass. For discovery, it is required that the number of signal events in a mass window gives a p-value, calculated using Poisson statistics, less than than 3×10^{-7} , with a minimum of 5 events required. The mass window is defined such that it contains 95% of the signal peak after resolution effects. This strategy leads to conservative estimates at high luminosity for Z' production at low mass due to large background levels, but preserves discovery sensitivity at high mass where background is minimal.

The discovery reach in the electron and muon channels is shown in Fig. 23. In both cases, the leading order cross section times branching ratio for various Z' models is also shown. In the electron channel, a 5.1 TeV Z'_{SSM} in the sequential standard model (SSM) can be discovered with 300 fb^{-1} of 14 TeV data. A 5 TeV Z'_η can be discovered with 1000 fb^{-1} of 14 TeV data. In the muon channel, Z'_ψ with a mass of 5 TeV can be discovered with approximately 900 fb^{-1} . These results are in good agreement with estimates of discovery potential prior to LHC operations [49].

6.2 Searches for Monoleptons+MET

In searches for new physics involving a high p_T lepton ($\ell = e, \mu$) and missing energy, two different models are considered for extrapolation to HL-LHC: the SSM W' [51] and a dark matter effective theory [52, 53]. In the SSM, the W' boson is considered to be a heavy analog of the SM W boson and thus can decay into a lepton and a neutrino, the latter giving rise to missing transverse energy as the observable detector signature. The branching fraction is expected to be 8% for each leptonic channel. In the dark matter model, a pair of dark matter particles (χ) are produced in association with a lepton and a neutrino deriving from an intermediate standard model W. Depending on the couplings (vector or axial-vector type), a scenario with constructive ($\xi = -1$) or destructive ($\xi = +1$) interference would be possible. Both signatures result in an excess of events in the transverse mass (M_T) spectrum.

The estimate of discovery reach is based on the 8 TeV search performed by CMS [54]. The signal acceptance at 14 TeV is assumed to be the same as at 8 TeV, which for W' masses ranging from 0.5 TeV to 2.5 TeV was found to be around 70% with a variation of $\pm 5\%$ in both channels,

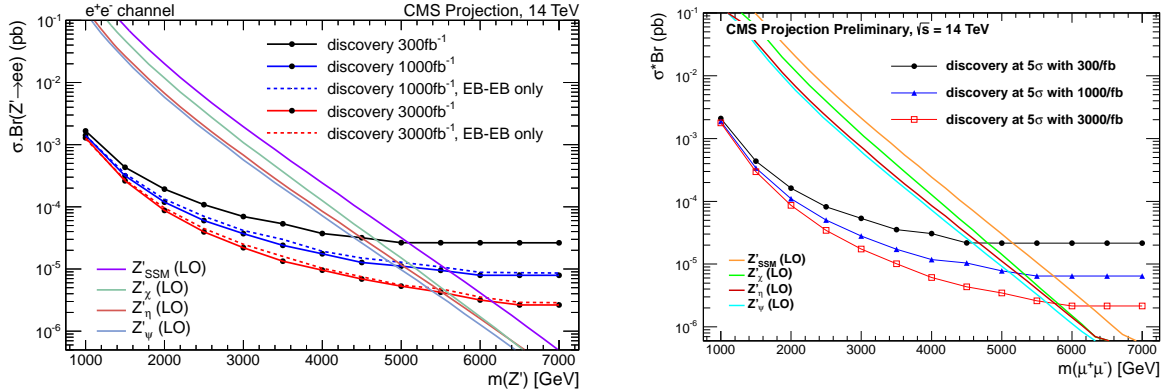


Figure 23: The minimum cross section times branching ratio for discovery as function of dielectron (left) and dimuon (right) mass for various luminosity scenarios. For the dielectron search, various luminosity and detector scenarios are considered, where the “EB-EB only” lines represent the reduced acceptance scenario in which electrons are reconstructed in the ECAL barrel only.

including 90% geometrical acceptance. The primary source of background is the off-peak, high transverse mass tail of the Standard Model $W \rightarrow \ell\nu$ decays. Other backgrounds are negligible at high M_T , which is the dominant region to set the upper limits on the model parameters. The background predictions are based on simulations up to very high transverse masses. Both signal and background are generated using MADGRAPH 4.5.1.

The signal parameter in case of a discovery is determined using the profile likelihood method by generating toy experiments. To assume a discovery, the median likelihood is required to be less than 5σ . The electron and muon channel are treated separately and their likelihoods are combined.

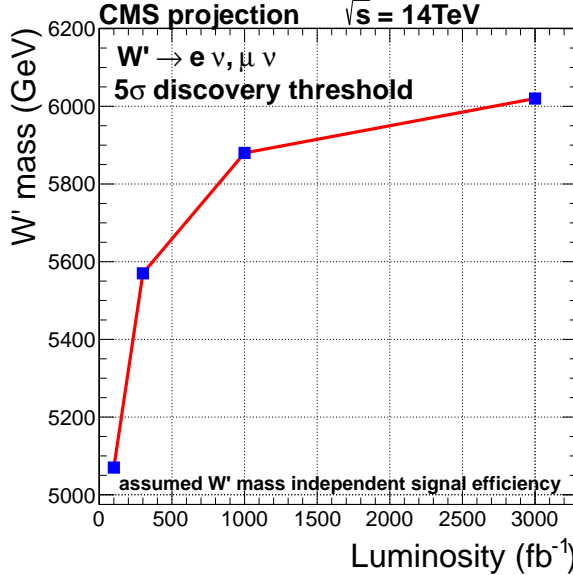


Figure 24: Projection of the 5σ discovery reach for $\sqrt{s} = 14$ TeV for the sequential standard model W' .

The resulting discovery sensitivity on the W' mass as a function of integrated luminosity is

shown in Fig. 24 for the combination of electron and muon channels. Given 3000 fb^{-1} of data, it is possible to discover a W' with a mass up to 6 TeV. For high masses the sensitivity is affected by the center-of-mass energy due to the growing fraction of W' bosons produced off-shell. The extrapolation assumes that lepton reconstruction and, in particular, isolation efficiency are not affected by increased pile-up, based on the observation of flat efficiency in events from data with up to 50 vertices. The W' cross sections are NNLO with a mass dependent k-factor.

The same event selection optimized for SSM W' can be used to search for pair-produced dark matter particles. Detailed studies at 8 TeV using this method have shown the signal efficiency to be 60% (10%) in the case of constructive (destructive) interference [55]. Applying this same procedure to the 14 TeV lepton + E_T^{miss} final state, the discovery reach relative to Λ , the scale of the effective interaction for associated dark matter pair production, is shown in Fig. 25. Signals with $\Lambda < 1.4$ TeV could be discovered in the case of destructive interference ($\xi = +1$) with an integrated luminosity of 3000 fb^{-1} . For $\xi = -1$, values up to $\Lambda = 2.3$ TeV lie within the sensitivity of the experiment. The discovery reach on the parameter Λ can be translated to a nucleon cross section as shown in Fig. 25 (right) for $M_\chi = 10 \text{ GeV}$ considering a vector or axial-vector coupling.

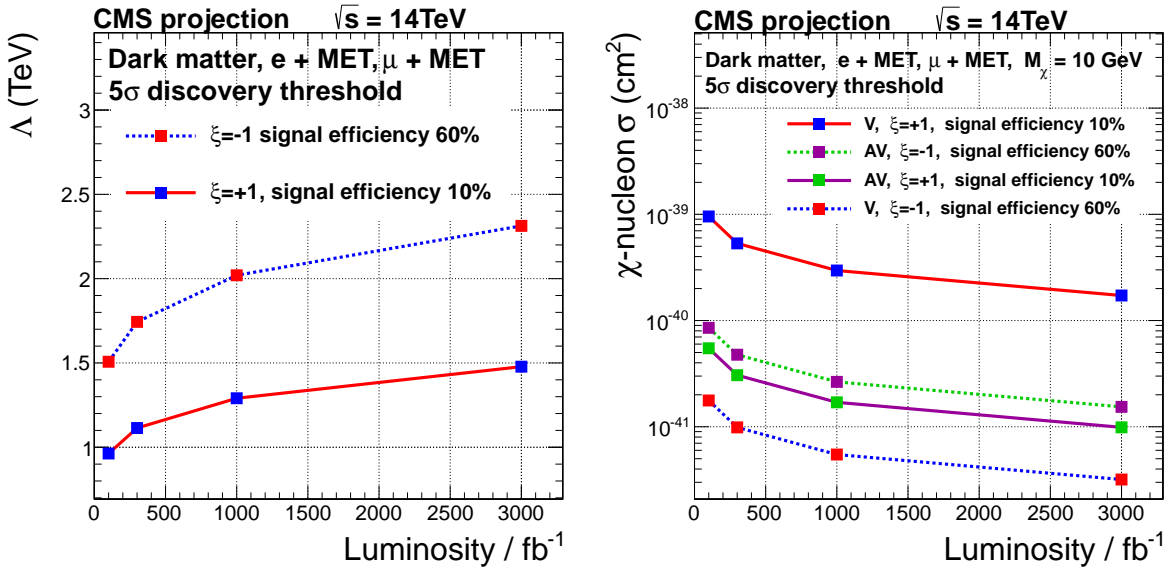


Figure 25: Projection of the discovery reach on Λ (left) and the dark matter-nucleon cross section (right) for the pair-produced dark matter model at $\sqrt{s} = 14 \text{ TeV}$ and a variety of luminosity scenarios. The discovery threshold is 5σ .

6.3 Searches for Heavy Stable Charged Particles

CMS has conducted searches for heavy stable charged particles (HSCP) produced in pp collisions at $\sqrt{s} = 7$ and 8 TeV , with integrated luminosities of 5.0 fb^{-1} and 18.8 fb^{-1} respectively, the results of which are presented in [56]. These searches present the most stringent limits to date on long-lived gluinos, scalar top quarks, and scalar τ leptons. The signatures utilized include long time-of-flight to the outer muon system and anomalously large energy deposition in the inner tracker, and the existing results are presented for each separately and in combination.

The sensitivity of these searches in the HL-LHC era is projected by scaling the results of the 8 TeV searches. Unlike many conventional searches, where backgrounds arise from irreducible physical processes, the background to these searches comes primarily from instrumental ef-

fects. It is therefore assumed that the backgrounds scale linearly with integrated luminosity, resulting in a constant signal over background ratio. By scaling the signal yields linearly with integrated luminosity from the 8 TeV result, a conservative assumption about the signal acceptance is introduced, since 14 TeV kinematics are expected to yield increased acceptance. Several changes are accounted for in LHC and detector operating conditions anticipated in the future. First, since the LHC has operated at 50 ns bunch spacing to date, the 8 TeV search was able to utilize a wide muon trigger time window, accepting candidates that arrive one LHC bunch-crossing after the collision. The LHC is expected to run with 25 ns bunch-spacing from 2015 onwards, resulting in a reduced trigger time window, so the signal efficiency used in these projections has been adjusted, based on fully simulated 8 TeV Monte-Carlo events. Secondly, the current dE/dx measurement relies on analog readout of the CMS Tracker, which will almost certainly not be possible after the CMS Tracker is upgraded during LS3. To account for this, the sensitivity with 3000 fb^{-1} is presented based on the combination of long time-of-flight and highly ionizing signatures, corresponding to an assumption that the dE/dx performance remains unchanged, and the sensitivity using the long time-of-flight signature alone, corresponding to an assumption that dE/dx measurements cannot be performed with the upgraded CMS Tracker.

These assumptions allow us to rescale the results of [56] to both higher center of mass energy and integrated luminosity with little difficulty. The results of this exercise are presented in terms of cross section reach defined as the cross section for which an observed signal is expected with a significance of at least 5 standard deviations (5σ). Figures 26 and 27 show the expected reach as a function of HSCP mass for hadron-like HSCP (stops and gluinos) and for lepton-like staus (direct and inclusive production), respectively.

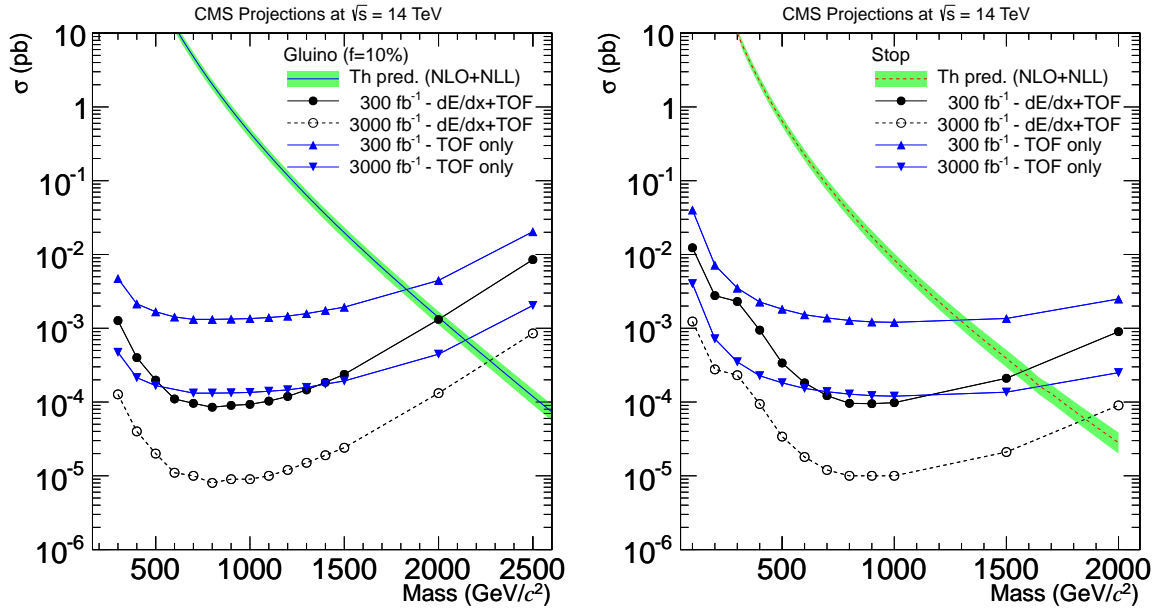


Figure 26: Minimum cross sections for an expected signal significance of 5 standard deviations. The signal models considered are the pair production of gluinos (left) and of stops (right).

The results show that the additional integrated luminosity will allow us to be sensitive to long-lived particles produced with a cross sections at least one order of magnitude lower than what has been excluded by [56]. It should be noted that the models considered in this search are simple benchmarks and the search for long-lived particles even in the already excluded mass

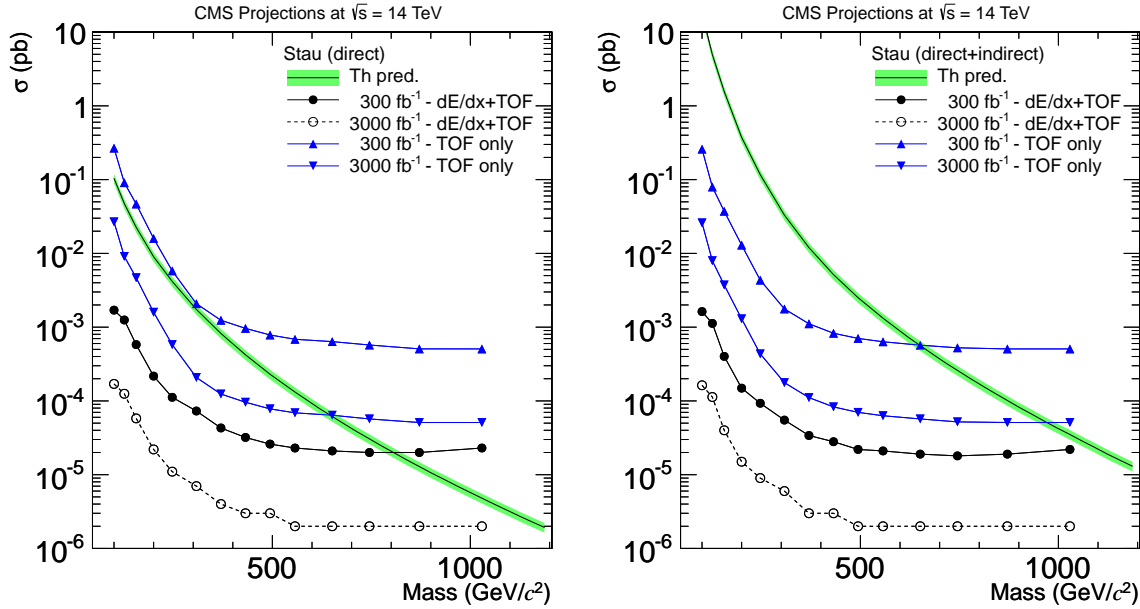


Figure 27: Minimum cross sections for an expected signal significance of 5 standard deviations. The signal models considered are the direct pair production of staus (left) and direct+indirect production of staus (right) in the context of GMSB.

range must be continued. This is because the exclusion results rely entirely on theoretical cross section predictions made in the context of a given model (e.g., Split SUSY, GMSB), while the analysis itself is signature-based and mostly decoupled from any given theoretical model. For example, it is known from past studies [57] that the sensitivity to lepton-like HSCPs in Universal Extra Dimension (UED) models is significantly less due to their lower production cross sections. The cross section limits should therefore be pushed as low as possible regardless of the excluded mass range as interpreted in the context of a few popular benchmark models.

6.4 Search for Heavy Vector-like Charge 2/3 Quarks

Vector-like quarks differ from SM quarks in their electroweak couplings. Whereas SM quarks have a V-A coupling to the W boson, i.e. their left and right-handed states couple differently to the W boson, vector-like quarks have only vector coupling to the W boson. One can thus write a mass term for them that does not violate gauge invariance without the need for a Yukawa coupling to the Higgs boson. Vector-like quarks are predicted, for example, by Little Higgs models [58, 59]. They can cancel the diverging contributions of top quark loops to the Higgs boson mass offering an alternative solution to the hierarchy problem.

We search for a vector-like T quark with charge +2/3, which is pair produced together with its antiquark in proton-proton collisions through the strong interaction. Thus its production cross section can be calculated using perturbative QCD. The T quark can decay into three different final states: bW, tZ, or tH. If it is an electroweak singlet the branching fractions are predicted to be 50% into bW and 25% each into tZ and tH [60]. At low masses the tZ and tH modes are kinematically suppressed. All T quark decays produce final states with b quarks and W bosons. Signal events therefore have large numbers of jets from b-quarks and hadronic W, Z, or H boson decays. For large T quark masses it becomes likely that the jets from one or more boson decay are not resolved which gives rise to jets that have substructure and a large invariant mass.

This sensitivity is based on an estimate on the T quark search carried out by CMS based on 19.6 fb^{-1} of pp collision data collected at a center of mass energy of 8 TeV [61]. This search considers eight channels which differ in their selection criteria. All require at least one electron or muon, together with a number of jets, which may be identified as originating from a b-quark or a boosted W or Z. The same selections are used for the projection to HL-LHC, with one simplification. For the single lepton channels, the 8 TeV results are based on the full spectrum of a boosted decision tree discriminant. Here, the same BDT discriminant is used, but simply accept events above a threshold, that was optimized for the expected significance.

In order to compute the expected sensitivity for pp-collisions at $\sqrt{s} = 14 \text{ TeV}$, the same selection efficiencies are used for signal and background as for the CMS analysis for $\sqrt{s} = 8 \text{ TeV}$. The signal yields are scaled using the calculated cross section from HATHOR. The backgrounds are scaled by the ratio of their NLO cross section. For the W+jets background this is 1.8, for the t̄t background it is 3.9, for the t̄tW background it is 3.3, and for the t̄tZ background it is 4.8. All other backgrounds are scaled by a factor 3. All yields are scaled proportionally to integrated luminosity assumed.

A simplified treatment of systematic uncertainties is applied. A flat 30% uncertainty is applied to the background yields in the multilepton channels. In the single lepton channels a 10% uncertainty is assigned to the t̄t background and 50% uncertainty to all other backgrounds. When estimating the sensitivity the background estimate is increased by the size of the uncertainties.

To determine the sensitivity, 10000 random pseudoexperiments are generated based on the expected number of signal and background events in each channel. For each channel i in each pseudoexperiment the p-value p_i is determined for the observed number of events under the background only hypothesis. The combined p-value of all channels is then computed, $P = k \sum_{i=0}^{n-1} (-\ln k^i / i!)$, where $k = \prod_{i=1}^n p_i$ and n is the number of channels to be combined.

Figure 28 shows plots of the discoverable T quark pair production cross section as a function of T quark mass, for the nominal branching fractions of 50%/25%/25% to bW/tZ/tH. The sensitivity is not expected to vary substantially if the branching fractions deviate from the nominal values. For the CMS analysis at $\sqrt{s} = 8 \text{ TeV}$ the mass limits vary inside a 100 GeV interval for any combination of branching fractions. At 14 TeV, T quarks with mass below 1 TeV could be discovered with 300 fb^{-1} of data, with the discovery reach extending to nearly 1.2 TeV with 3000 fb^{-1} accumulated.

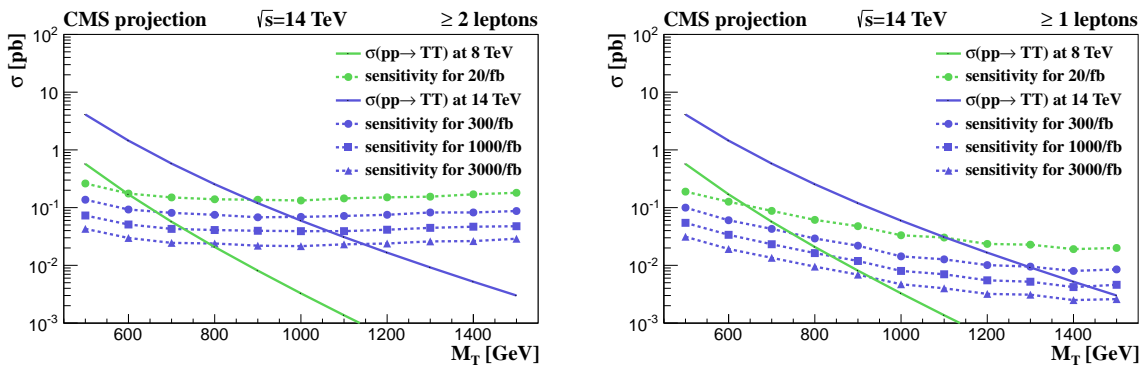


Figure 28: Expected sensitivity for a T quark pair production signal in the multilepton channels only (left), and in all channels combined (right).

7 Top Quark Physics

The copious production of top quarks at the LHC, together with the excellent performance and understanding of the CMS detector, allows for studies of top quark properties and the mechanism of their production and decay with unprecedented detail and precision. Already with the 7 TeV LHC dataset, CMS has caught up with the Tevatron and surpassed both D0 and CDF in precision for key measurements such as that of the top quark mass where CMS has now achieved the most precise single results in each of the $t\bar{t}$ decay modes. Similarly, the $t\bar{t}$ and single-top production cross sections have been determined with a relative precision that is challenging the theoretical predictions in differential cross section measurements.

With the addition of 8 TeV data, CMS top physics measurements will break new ground across the entire program. Many goals here range from measuring cross sections and rare production processes, to a further improvement in the mass determination, the exploration of its spin and decay properties, the V_{tb} coupling, the refinement of the strategies to use the top as a search tool, etc. In the process of covering this, there are many bread and butter measurements that will be obtained. One example is the determination of α_s using the full NNLO+NNLL calculation of the $t\bar{t}$ cross section [62], for different PDF sets, as shown in Fig. 29 (left). Preliminary results at 8 TeV confirm earlier observations at 7 TeV [63] revealing clear differences between data and NLO MC predictions in key differential kinematic distributions such as the transverse momentum distribution of top quarks in $t\bar{t}$ events, shown in Fig. 29 (right). Full NNLO differential calculations, that should become available in the next years, may resolve some of the current discrepancies. In the meantime, detailed study of the pre-LS1 dataset continues to constrain (gluon) PDFs, and improve understanding of the modeling of additional jets from ISR and FSR in $t\bar{t}$ events. Improved theoretical tools, including NLO parton-shower matched simulation, are being commissioned and are expected to play an important role. These new tools and studies are crucial to lay a solid foundation for post-LS1 analysis of 14 TeV data.

With 300 fb^{-1} at 14 TeV CMS will record some 50 million $t\bar{t}$ events in the lepton+jets channel, and about 10 million events in the dilepton channel. In addition, some 15 million events of single-top production can be collected in the various channels with leptonic triggers.

With these large samples we can study very rare top decays like those induced by flavor-changing neutral currents (FCNC). These decays occur in the SM only in quantum-loop corrections with tiny branching fractions (10^{-14}) and their observation would be a clear signal of new physics. There are models of new physics that predict branching fractions as high as 10^{-4} [65, 66]. As an example, an extrapolation from the current search for $t \rightarrow Zq$ decays [67] yields sensitivities around 10^{-5} , in the interesting range for SUSY [68]. Sensitivities in the range 10^{-5} – 10^{-4} (and higher with HL-LHC) are expected for other FCNC decays $q\gamma$ and qg [30]. High luminosity is also necessary for precise studies of the tWb vertex which can be performed in terms of an effective Lagrangian [69] requiring a common analysis of $t\bar{t}$ and single-top production.

The study of the associated production of top with γ , W and Z will give access to the top coupling to bosons. First evidence of $t\bar{t}Z$ and $t\bar{t}W$ production has been recently observed [70], opening the road to precise measurements in this area. A more difficult analysis is the study of the $t\bar{t}H$ associated production where a very good control of the background will be needed to extract the coupling with precision. In addition, it is key to be able to keep systematic uncertainties under control, which would for example require excellent understanding of the b-tagging performance with the upgraded CMS detector. As shown in Sec. 4, with the HL-LHC a measurement of the top-Yukawa coupling with a precision better than 10% is expected.

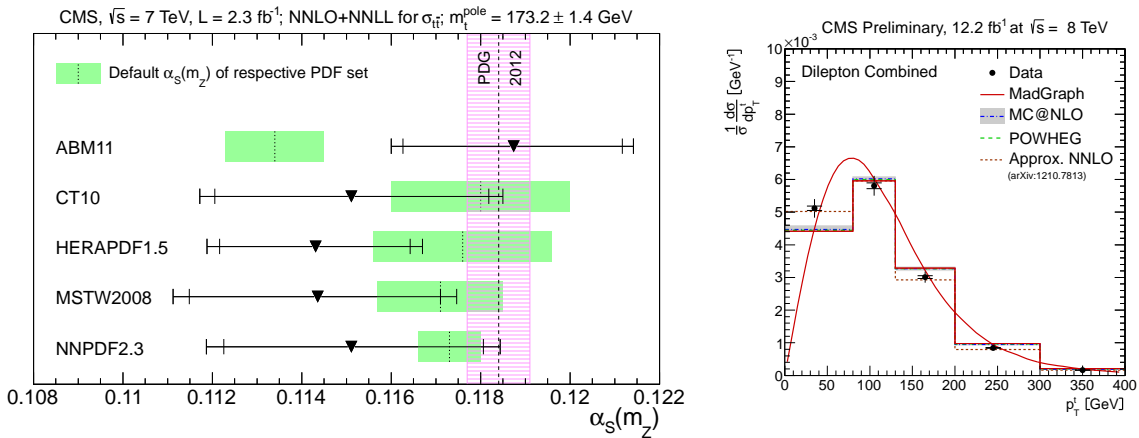


Figure 29: Left: Results obtained for $\alpha_s(m_Z)$ from the measured $t\bar{t}$ cross section together with the prediction at NNLO+NNLL using different NNLO PDF sets. The inner error bars include the uncertainties on the measured cross section and on the LHC beam energy as well as the PDF and scale uncertainties on the predicted cross section. The outer error bars additionally account for the uncertainty on m_{top} . For comparison, the latest $\alpha_s(m_Z)$ world average with its uncertainty is shown as a hatched band. For each PDF set, the default $\alpha_s(m_Z)$ value and its uncertainty are indicated using a dotted line and a shaded band (from [62]). Right: Normalised differential $t\bar{t}$ production cross section as a function of the p_T^t of the top quarks. The inner (outer) error bars indicate the statistical (combined statistical and systematic) uncertainty. The measurements are compared to predictions from MADGRAPH +PYTHIA, POWHEG+PYTHIA, MC@NLO+HERWIG, and to an approximate NNLO calculation. The MADGRAPH +PYTHIA prediction is shown both as a curve and as a binned histogram (from [64]).

New physics coupled to the third generation can affect $t\bar{t}$ production and give rise to bumps and distortions in the $t\bar{t}$ invariant mass spectrum. High statistics enhances the sensitivity to distortions to the expected shape, and will extend the range to higher mass resonances. The study of asymmetries is particularly promising for high-luminosity measurements, since many systematic effects cancel in the ratios. New physics in $t\bar{t}$ production can be unveiled by studying charge asymmetries and spin correlations [71–73].

The very large statistics sample will open also the possibility to exploit new methods to extract more accurate values of the top mass with exclusive decays like $t \rightarrow b \rightarrow J/\psi$, or exploiting the shape of the lepton spectrum. Another interesting technique which requires high statistics is the measurement of the top mass using the B hadron decay length [74]. A new development pioneered by CMS is the measurement of the top mass as a function of kinematic properties of the $t\bar{t}$ bar events [75], and the measurement of the difference between the top quark and anti-quarks [76, 77]. In addition to a test of CPT invariance the latter measurement is a test of soft non-perturbative QCD effects that may affect top quark and anti-quark decays differently. With further study and sufficiently large statistics these methods can shed light on the dependency of the top mass on color reconnection and other QCD effects. An improved understanding of the interpretation of the top mass measurements is particularly important in view of a very high precision measurement of the W mass, and since the Higgs boson mass is now known.

8 Electroweak Physics

The goals of the CMS electroweak program are at least threefold:

- To test the standard model theory of electroweak symmetry breaking at the TeV scale via a comprehensive portfolio of (multi)boson production measurements;
- To improve upon traditional precision electroweak observables;
- To produce precision PDF constraints and tests of perturbative QCD/electroweak predictions.

8.1 Multiboson production

The observed Higgs boson is a very attractive explanation for mass and electroweak symmetry breaking, however what is not yet known to any precision is whether it plays the desired role of completely restoring unitarity to the gauge-boson interaction sector of the SM, or whether other physics is also participating. The classic test is to measure $W_L - W_L$ scattering via vector-boson fusion (VBF) production of WW pairs. In addition, VV scattering is potentially linked also, in the context of electroweak-gauge-invariant effective field theory, with other triple and quartic gauge interactions (TGC and QGC), and hence as many sensitive multiboson final states as possible should be studied. Examples of this rich sector include:

- Differential cross sections of inclusive diboson production, in all combinations (especially at the highest p_T or mass);
- VBF diboson production (a recent search for exclusive photoproduction of WW [78] is already an example of this which probes the $WW\gamma\gamma$ QGC);
- VBF single boson production (already examined for Z production at 7 TeV [79]) ;
- triboson production (not yet observed at the LHC).

These measurements typically involve processes with small cross sections, and the most valuable information is contained in the high-mass, high-momentum tails of their distributions. Their study will therefore be relevant throughout the 14 TeV era and at the highest integrated luminosities. They will benefit from detector upgrades in similar fashion to the Higgs program, which examines most all of the same final states. Of particular value will be VBF dijet triggering and reconstruction, crucial to isolating VV scattering events. Another important upgrade impact will be preserving the capability, through precision tracking and higher-granularity calorimetry, of the analysis of jet substructure. At the TeV scale, hadronic decays of bosons are exhibited in the detector as dijets merged into a single jet. Analysis at the particle level of these jets (“W/Z-tagging”) is critical to identify VV (or VVV) candidates.

8.2 Precision constraints of the electroweak theory

In the domain of precision electroweak data, the statistical power is clear: CMS has already recorded W samples far in excess of the Tevatron, and Z dilepton samples in excess of LEP 1. If systematic uncertainties can be appropriately constrained, then progress can be made in the understanding of the W mass (through kinematic distributions of leptonic W decays) and the effective weak mixing angle (through angular distributions of dileptonic Z decays).

In the case of the W mass, the appropriate statistical power is known to be present in the Run 1 data alone. However the systematic limitations from PDFs (and possibly the detector) may only find solution in higher statistics samples and an upgraded detector in Run 2. For the weak-mixing angle, it is known from the first successful CMS measurement [80] that the limitations are from statistics, PDFs, and tracker alignment. With the Run 2 data the statistical uncertainty will be comparable to the world-average uncertainty; it then remains to improve tracker alignment and PDFs, again exploiting higher Run 2 statistics, and the improved capabilities of tracking with pixel upgrades.

8.3 Constraints of PDFs and validation of perturbative predictions

Finally, in the domain of precision tests of PDFs and perturbative predictions, there are several samples of electroweak boson production relevant to validating our understanding of standard model predictions generally:

- Precision understanding of W or Z production at the LHC requires improved determination of gluon, strange, and charm quark PDFs, as they play a much stronger role at LHC energies than at the Tevatron. In addition, further progress must be made with valence quarks, and over a broader range in Björken x . Similarly to the Tevatron, however, W and Z samples can be boot-strapped to measure these PDFs in situ. For example, the recent CMS W+c cross section measurement [81] provides a strange PDF constraint which is already starting to be competitive with fixed-target neutrino data, and the CMS W lepton charge asymmetry measurements [82, 83] already over-constrain the u/d PDF ratio compared to pre-LHC PDFs.
- A new generation of next-to-leading-order QCD, parton-shower matched (NLO+PS) simulations are now being commissioned (Sherpa 2.0, aMC@NLO, POWHEG), which give true NLO+PS-matched predictions for $2 \rightarrow 3, 4, 5, 6$ -body processes; they will be crucial to understand 6-fermion final states like VV scattering. In the coming years, next-to-next-to-leading order (NNLO) QCD predictions for these processes are also expected to mature, demanding another round of confrontation with experiment.
- At the TeV scale, radiative and loop corrections due to W, Z, or photon emission leads to next-to-leading order electroweak corrections comparable to NLO QCD. These effects must be isolated (typically in the highest mass Drell-Yan or diboson production differential cross sections), measured, and compared with NLO electroweak (possibly in concert with NLO or NNLO QCD corrections) predictions where available.

This is a broad and ongoing program of cross section measurement which evolves with beam energy and luminosity, as the relevant higher-order effects are typically strongly energy-dependent. To understand the heavy-flavor PDFs, a dedicated triggering strategy must be adopted, with detector upgrade requirements similar to the $H \rightarrow bb$ analysis.

9 Heavy Ion Physics

The primary goal of relativistic heavy-ion physics is to study the phases of nuclear matter and the transitions between them. Of particular interest is the characterization of the extremely high energy-density phase, the quark-gluon plasma (QGP), in which the quarks and gluons comprising the atomic nuclei are deconfined and chiral symmetry is restored. Owing to its high center-of-mass energy and high luminosity, the LHC is in a unique position to explore the properties of the QGP using rare processes, such as the production of heavy quarkonium states, jets of different flavors, electroweak bosons, and the correlations between these rare probes of the medium produced in the nuclear collisions. CMS is ideally suited to carry out this program, due to its large acceptance, high-rate triggering and data acquisition capabilities. The high luminosity regime of the LHC gives the opportunity to explore the QGP phase with rare probes and the Heavy Ion community is proposing to collect 10 nb^{-1} of lead-lead (PbPb) collisions. This number is used in this document to evaluate the physics prospects of the CMS heavy-ion program.

9.1 Proposed strategy

By the end of LS2, CMS will have completed its first upgrade phase including a new pixel vertex detector with larger redundancy, an upgraded trigger, an extension of the forward muon system and a refurbishment of the hadron calorimeter electronics including the replacement of the PMTs of the forward hadron calorimeter. The selectivity of high- p_T jets at L1 will be augmented by implementing a subtraction for the underlying event and the DAQ upgrade will allow to increase the bandwidth of the tracker detector. The combination of these upgrades will raise the maximum PbPb interaction rate that can be sampled by CMS detector from about 5 kHz, as observed in Run 1 to above 50 kHz. This will allow the CMS heavy-ion program to fully exploit the high luminosity heavy-ion running, after the LHC collimator upgrades are completed in LS2.

During LS3, CMS will upgrade the inner tracker and will make many other changes to sub-detectors, trigger and data acquisition systems. These improvements will further augment the capabilities of the CMS experiment to study heavy-ion collisions by increasing the track reconstruction efficiencies and acceptance among other improvements.

9.2 Plans for heavy-ion physics in the HL-LHC era

In case of a successful dispersion collimator installation in the LHC, and stochastic cooling tests in the PS/SPS in the LS2, the LHC is expected to reach its currently maximum foreseen instantaneous PbPb luminosity of $\approx 6 \times 10^{-27} \text{ cm}^{-2} \text{ s}^{-1}$, providing a 50 kHz collision rate at the nominal PbPb center-of-mass energy of 5.5 TeV. With these running conditions the heavy-ion community is proposing to collect a total of 10 nb^{-1} , which is approximately 60 times more than what is presently available, in terms of number of events sampled, with the additional benefit of a higher center-of-mass energy, which in turn leads to higher production cross sections of hard probes.

This increase in collision energy and luminosity will again necessitate recording reference pp and pPb data, with a center-of-mass energy and statistics corresponding to the ones of the PbPb dataset.

One of the most important questions is to precisely quantify the parton energy loss in the hot and strongly interacting medium produced in PbPb collisions. Of particular interest are the parton flavor dependence and the path length dependence of this phenomenon, which was for the first time directly observed as an imbalance of the energies of back-to-back jets [84, 85]. Such an imbalance is also observed in isolated-photon+jet pairs [86]. Expanding these initial observations to precision measurements, especially measurements of differential parton flavor or in the azimuthal angle relative to the reaction plane, to study the path length dependence will require significantly higher event rates.

Table 5 illustrates the expected number of events containing the various physics signatures of interest for high-precision parton energy loss studies in a 10 nb^{-1} PbPb collision sample. The estimated numbers are based on the observed rates in the Run 1 dataset.

A first set of studies of the quark flavor dependence of parton energy loss using jets arising from bottom quark fragmentation or three jet events will become feasible when the LHC energy is raised to 14 TeV, as illustrated by the corresponding studies presented below. These analyses were conducted to study the performance impact of the L1 calorimeter trigger upgrade on CMS heavy ion data taking.

The ideal measurement in the b-jet channel would be a measurement of the dijet asymmetry for

Table 5: Expected hard probe event rates in PbPb collisions at the LHC (2015-2017) and HL-LHC (2019-2025) heavy-ion running. The estimate is derived from the data collected in Run 1 of the LHC.

	2010–2013 2.76 TeV 160 nb^{-1}	2015–2017 5.5 TeV 0.3–1.5 nb^{-1}	2019–2025 5.5 TeV ~ 10 nb^{-1}
Jet p_T reach (GeV/c)	~ 300	~ 500	~ 1000
Track p_T reach (GeV/c)	~ 100	~ 160	~ 300
Dijet ($p_{T,1} > 120\text{GeV}/c$)	50k	$\sim 300\text{k} - 1.5\text{M}$	$\sim 10\text{M}$
b-jet ($p_T > 120\text{GeV}/c$)	~ 500	$\sim 4\text{k} - 21\text{k}$	$\sim 140\text{k}$
Isolated γ ($p_T^\gamma > 60\text{GeV}/c$)	$\sim 1.5\text{k}$	$\sim 9\text{k} - 45\text{k}$	$\sim 300\text{k}$
Isolated γ ($p_T^\gamma > 120\text{GeV}/c$)	—	$\sim 300 - 1.5\text{k}$	$\sim 10\text{k}$
W ($p_T^W > 50\text{GeV}/c$)	~ 100	$\sim 600 - 3\text{k}$	$\sim 20\text{k}$
Z ($p_T^W > 50\text{GeV}/c$)	~ 10	$\sim 60 - 300$	$\sim 2\text{k}$
$t\bar{t} \rightarrow l^+l^- b\bar{b}$ MET	$\sim \mathcal{O}(10)$	$\sim 100 - 200$	~ 600

doubly tagged b jets, where we expect systematic uncertainties to be small, and to mostly cancel with respect to the corresponding light-quark jet measurements. The rate of doubly tagged b jets has been estimated based on the number of inclusive dijets in the 2011 sample. The b-jet-to-inclusive-jet ratio was measured to be approximately 0.03 in pp collisions at 7 TeV, as well as in 2.76 TeV PbPb collisions, with significantly larger uncertainties in the latter case. Of these b jets only about 20% will be produced back-to-back with another b jet, in the so-called flavor-creation mode. Using a simple secondary-vertex tagger, one can achieve about 50% tagging efficiency in PbPb. For doubly tagged jets, then, one only obtains a tagging efficiency of 25%, but with a purity close to unity. Assuming x_T scaling with an exponent of $n = 4.5$, the yield of jets at fixed p_T increases by a factor of 5 for the increased collision energy expected in 2015.

The dijet asymmetry A_J is defined as the difference between the leading and subleading jet transverse momenta, divided by their sum. The A_J distribution for doubly tagged b jets is estimated from the inclusive jet A_J distribution, scaling the uncertainties to those expected from 1.5 nb^{-1} of data at 5.5 TeV, with a tagging efficiency of 25%. This distribution is shown in Fig. 30 for the 10% most-central PbPb events. The kinematic selection on the leading and sub-leading jets are $p_T > 100\text{ GeV}/c$ requires $p_T > 30\text{ GeV}/c$, respectively, for jets in $|\eta| < 2$.

Events with three or more jets in the final state originate from hard gluon radiation and other higher-order QCD processes. A measurement of the inclusive 3-jet to 2-jet cross section ratio (R_{32}) is an interesting testing ground of pQCD, with possible modification of parton-shower and gluon jet quenching in QGP, because major systematic uncertainties such as jet energy scale, reconstruction efficiency and integrated luminosity largely cancel. The expected number of 3-jet events at 5.5 TeV is estimated based on the observed statistics in the 2011 data sample, in which we recorded about 106 3-jet events and 8225 dijet events, with all jets having $p_T > 100\text{ GeV}/c$. The ratio from PYTHIA events, with uncertainties scaled to the expected 2015 statistics, is shown in Fig. 31.

While the measurements detailed above will become accessible already based on the 1.5 nb^{-1} expected to be recorded in the next run of the LHC, extracting the full path length dependence of parton energy loss in these channels by an analysis differential in the angle with respect to the reaction plane will require another increase of event rate by a factor of 5–10, which will be achieved in the High Luminosity Ion running period of the LHC.

Other important channels to study parton energy loss, which should be possible at the HL-LHC

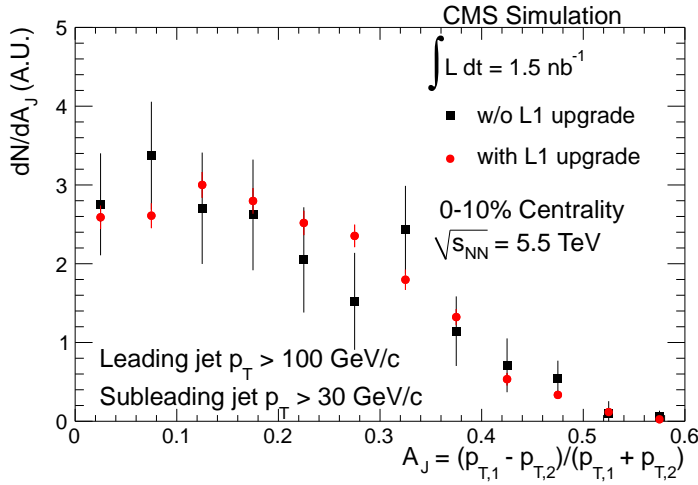


Figure 30: A_J distribution for doubly tagged b jets of $p_{T,1} > 100$ GeV/c, $p_{T,2} > 30$ GeV/c and $|\eta| < 2$ in the ten percent most central collisions expected in the 2015 PbPb Run.

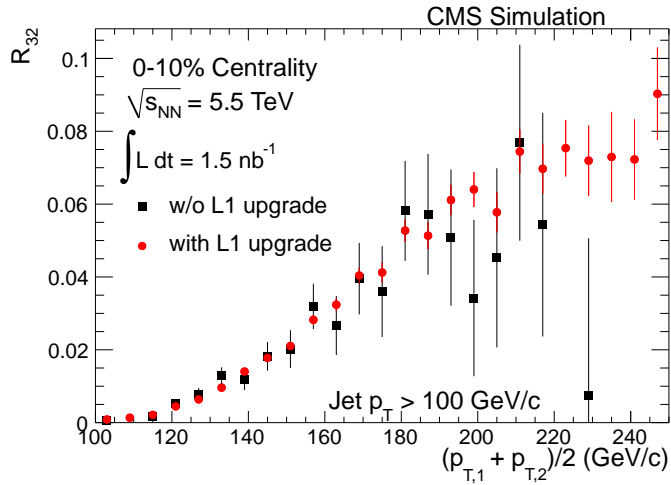


Figure 31: The ratio of 3-jet to 2-jet events (R_{32}) as a function of the average p_T of the two leading jets for $p_T > 100$ GeV/c in the 10% most-central collisions expected in the 2015 PbPb Run.

are the γ +jet and Z+jet energy balance. Comparing Z+jet and γ +jet observables to inclusive jets will allow to start separating quark jets from gluon jets. The collected number of γ +jet events will be sufficient to study the jet quenching as a function of the reaction plane.

The suppression of quarkonium states, such as the Y family members, is another interesting signal of the QCD phase transition occurring in heavy-ion collisions. The dependence of this suppression on the collision centrality is especially interesting, where the measurement is severely limited by the number of peripheral collisions. A large statistics dataset would allow CMS to precisely map out the centrality dependence as well as conduct a more differential, reaction-plane dependent study.

The list of physics studies that can be performed with a 10 nb^{-1} data sample will include:

- Detailed measurements of multijet correlations, shedding light on gluon versus quark

- jet quenching;
- Differential studies of photon+jet correlations as a function of photon p_T , event centrality or the reaction plane orientation;
- Detailed measurements of Z+jet correlations, with up to 3000 and 600 Z bosons having transverse momentum above 50 and 100 GeV/ c , respectively;
- Differential measurement, such as azimuthal correlations for the rarest probes ($\psi(2S)$);
- Multiobject correlations;
- Jet quenching studies up to the TeV scale;
- Precision measurements of the quarkonium suppression pattern.

The physics channels listed above are probably the most interesting topics in heavy-ion physics at the LHC today and in the future, and the CMS apparatus is especially well suited to study those, thanks to the excellent and flexible trigger, to the extended and precise muon system, to the high-coverage calorimetry, to the photon isolation, vertexing, and precise jet energy measurement capabilities. The high luminosity era of the LHC will mark the beginning of high-precision studies of the parton energy loss mechanism and the dynamics of the medium created in heavy-ion collisions.

10 Conclusions

The discovery of a Higgs boson last summer invigorated the field of particle physics and offered new insights as to where the next discoveries may occur. We believe that building on the success of this discovery by detailed characterization of the newly observed particle, elucidating the nature of EWSB mechanism, and continuing searches for physics beyond the standard model should therefore be the highest priority for high-energy physics in the next decade. One of the most important components of this quest is the exploitation of the full potential of the upgraded LHC. The HL-LHC upgrade will contribute greatly to our understanding of Nature and will allow us to carry out the above ambitious goals, along with a host of electroweak precision measurements, which will extend our sensitivity to new physics models.

The characterization of the newly discovered 125 GeV boson by precision measurements of its mass and tree-level couplings to fermions, W and Z bosons, as well as self-coupling, at the HL-LHC will allow us to prove that it is the SM Higgs boson or, if it is not, to uncover the true nature of the observed particle. In addition, precision measurement of the couplings of the Higgs to photons and gluons via quantum loops will provide sensitive probes for possible new physics beyond the SM. Continuation of searches for SUSY with massive squarks and gluinos, as well as for the superpartners of the third-generation quarks and electroweak bosons will either result in the finding of a “natural” solution to the hierarchy problem of the Standard Model or proving that this model is ultimately fine-tuned.

The discovery of the new boson was an immensely exciting and important event in humankind’s quest for the fundamental laws of physics. There is every reason to believe that more discoveries await us at the LHC. The rich physics program described above provides overwhelming justification for the upgrades of the CMS detector needed to exploit this magnificent and unique opportunity.

References

- [1] See <http://www.snowmass2013.org/tiki-index.php>.

- [2] W. J. Sterling, private communication.
- [3] CMS Collaboration, “CMS at the High-Energy Frontier. Contribution to the Update of the European Strategy for Particle Physics”, CMS Note CMS-NOTE-2012-006, (2012).
- [4] ATLAS Collaboration, “Observation of a new particle in the search for the Standard Model Higgs boson with the ATLAS detector at the LHC”, *Phys.Lett.* **B716** (2012) 1–29, doi:10.1016/j.physletb.2012.08.020, arXiv:1207.7214.
- [5] CMS Collaboration, “Observation of a new boson at a mass of 125 GeV with the CMS experiment at the LHC”, *Phys.Lett.* **B716** (2012) 30–61, doi:10.1016/j.physletb.2012.08.021, arXiv:1207.7235.
- [6] CMS Collaboration, “Updated measurements of the Higgs boson at 125 GeV in the two photon decay channel”, CMS Physics Analysis Summary CMS-PAS-HIG-13-001, (2013).
- [7] CMS Collaboration, “Properties of the Higgs-like boson in the decay $H \rightarrow ZZ \rightarrow 4l$ in pp collisions at $\sqrt{s} = 7$ and 8 TeV”, CMS Physics Analysis Summary CMS-PAS-HIG-13-002, (2013).
- [8] CMS Collaboration, “Update on the search for the standard model Higgs boson in pp collisions at the LHC decaying to $W+W-$ in the fully leptonic final state”, CMS Physics Analysis Summary CMS-PAS-HIG-13-003, (2013).
- [9] ATLAS Collaboration, “Measurements of Higgs boson production and couplings in diboson final states with the ATLAS detector at the LHC”, arXiv:1307.1427.
- [10] CMS Collaboration, “Search for the Standard-Model Higgs boson decaying to tau pairs in proton-proton collisions at $\sqrt{s} = 7$ and 8 TeV”, CMS Physics Analysis Summary CMS-PAS-HIG-13-004, (2013).
- [11] CMS Collaboration, “Search for the standard model Higgs boson produced in association with W or Z bosons and decaying to bottom quarks (LHC 2013)”, CMS Physics Analysis Summary CMS-PAS-HIG-13-012, (2013).
- [12] ATLAS Collaboration, “Search for the $b\bar{b}$ decay of the Standard Model Higgs boson in associated W/ZH production with the ATLAS detector”, ATLAS Conference Note ATLAS-CONF-2013-079, (2013).
- [13] ATLAS Collaboration, “Combined coupling measurements of the Higgs-like boson with the ATLAS detector using up to 25 fb^{-1} of proton-proton collision data”, ATLAS Conference Note ATLAS-CONF-2013-034, (2013).
- [14] CMS Collaboration, “Measurements of the properties of the new boson with a mass near 125 GeV”, CMS Physics Analysis Summary CMS-PAS-HIG-13-005, (2013).
- [15] CMS Collaboration, “On the mass and spin-parity of the Higgs boson candidate via its decays to Z boson pairs”, *Phys.Rev.Lett.* **110** (2013) 081803, arXiv:1212.6639.
- [16] ATLAS Collaboration, “Evidence for the spin-0 nature of the Higgs boson using ATLAS data”, arXiv:1307.1432.
- [17] CMS Collaboration, “CMS Technical Design Report for the Pixel Detector Upgrade”, CERN-LHCC-2012-016, (2012).

- [18] CMS Collaboration, “CMS Technical Design Report for the Phase 1 Upgrade of the Hadron Calorimeter”, CERN-LHCC-2012-015, (2012).
- [19] CMS Collaboration, “CMS Technical Design Report for the Level-1 Trigger Upgrade”, CERN-LHCC-2013-011, (2013).
- [20] CMS Collaboration, “Search for invisible Higgs decays in the VBF channel”, CMS Physics Analysis Summary CMS-PAS-HIG-13-013, (2013).
- [21] CMS Collaboration, “Search for invisible decays of a Higgs produced in association with a Z boson”, CMS Physics Analysis Summary CMS-PAS-HIG-13-018, (2013).
- [22] J. Baglio et al., “The measurement of the Higgs self-coupling at the LHC: theoretical status”, *JHEP* **04** (2013) 151, doi:10.1007/JHEP04(2013)151, arXiv:1212.5581.
- [23] CMS Collaboration, “Search for ttH production in events with $H \rightarrow \gamma\gamma$ at $\sqrt{s}=8$ TeV collisions”, CMS Physics Analysis Summary CMS-PAS-HIG-13-015, (2013).
- [24] CMS Collaboration, “Evidence for a particle decaying to W^+W^- in the fully leptonic final state in a standard model Higgs boson search in pp collisions at the LHC”, CMS Physics Analysis Summary CMS-PAS-HIG-12-042, (2013).
- [25] CMS Collaboration, “Search for the Standard Model Higgs Boson in $WH \rightarrow WWW \rightarrow 3\ell 3\nu$ Decays”, CMS Physics Analysis Summary CMS-PAS-HIG-13-009, (2013).
- [26] CMS Collaboration, “Search for the standard model Higgs boson decaying to tau pairs produced in association with a W or Z boson with the CMS experiment in pp collisions at $\text{sqrt}(s) = 7$ and 8 TeV”, CMS Physics Analysis Summary CMS-PAS-HIG-12-053, (2013).
- [27] CMS Collaboration, “Search for the standard model Higgs boson produced in association with W or Z bosons, and decaying to bottom quarks”, CMS Physics Analysis Summary CMS-PAS-HIG-12-044, (2013).
- [28] CMS Collaboration, “Search for the standard model Higgs boson produced in association with a top-quark pair in pp collisions at the LHC”, *JHEP* **05** (2013) 145, doi:10.1007/JHEP05(2013)145, arXiv:1303.0763.
- [29] CMS Collaboration, “Search for a Higgs boson decaying into a Z and a photon in pp collisions at $\text{sqrt}(s) = 7$ and 8 TeV”, arXiv:1307.5515. Submitted to *Phys. Lett. B*.
- [30] F. Gianotti, M. Mangano, T. Virdee et al., “Physics potential and experimental challenges of the LHC luminosity upgrade”, *Eur. Phys. J. C* **39** (2005) 293, doi:10.1140/epjc/s2004-02061-6.
- [31] T. Plehn and D. L. Rainwater, “Higgs decays to muons in weak boson fusion”, *Phys.Lett. B* **520** (2001) 108–114, doi:10.1016/S0370-2693(01)01157-1, arXiv:hep-ph/0107180.
- [32] T. Han and B. McElrath, “ $h \rightarrow \mu^+\mu^-$ via gluon fusion at the LHC”, *Phys.Lett. B* **528** (2002) 81–85, doi:10.1016/S0370-2693(02)01208-X, arXiv:hep-ph/0201023.
- [33] David, A. and Denner, A. and Duehrseen, M. et al., LHC Higgs Cross Section Working Group, “LHC HXSWG interim recommendations to explore the coupling structure of a Higgs-like particle”, arXiv:1209.0040.

- [34] CMS Collaboration, “Search for Supersymmetry in pp collisions at 8 TeV in events with a single lepton, multiple jets and b-tags”, CMS Physics Analysis Summary CMS-PAS-SUS-13-007, (2013).
- [35] CMS Collaboration, “Search for gluino mediated bottom- and top-squark production in multijet final states in pp collisions at 8 TeV”, arXiv:1305.2390.
- [36] CMS Collaboration, “Search for top-squark pair production in the single lepton final state in pp collisions at 8 TeV”, CMS Physics Analysis Summary CMS-PAS-SUS-13-011, (2013).
- [37] CMS Collaboration, “Search for SUSY in the same-sign dilepton final state”, CMS Physics Analysis Summary CMS-PAS-SUS-13-013, (2013).
- [38] CMS Collaboration, “Search for new physics in events with same-sign dileptons and b jets in pp collisions at $\sqrt{s} = 8$ TeV”, *JHEP* **1303** (2013) 037, doi:10.1007/JHEP03(2013)037, arXiv:1212.6194.
- [39] CMS Collaboration, “Search for electroweak production of charginos, neutralinos, and sleptons using leptonic final states in pp collisions at $\sqrt{s} = 8$ TeV”, CMS Physics Analysis Summary CMS-PAS-SUS-13-006, (2013).
- [40] W. Beenakker, R. Hopker, M. Spira, and P. Zerwas, “Squark and gluino production at hadron colliders”, *Nucl.Phys.* **B492** (1997) 51–103, doi:10.1016/S0550-3213(97)80027-2, arXiv:hep-ph/9610490.
- [41] W. Beenakker et al., “Stop production at hadron colliders”, *Nucl.Phys.* **B515** (1998) 3–14, doi:10.1016/S0550-3213(98)00014-5, arXiv:hep-ph/9710451.
- [42] W. Beenakker et al., “The Production of charginos / neutralinos and sleptons at hadron colliders”, *Phys.Rev.Lett.* **83** (1999) 3780–3783, doi:10.1103/PhysRevLett.83.3780, arXiv:hep-ph/9906298.
- [43] T. Sjöstrand, S. Mrenna, and P. Skands, “PYTHIA 6.4 physics and manual”, *JHEP* **05** (2006) 026, doi:10.1088/1126-6708/2006/05/026, arXiv:hep-ph/0603175.
- [44] R. Field, “Early LHC Underlying Event Data – Findings and Surprises”, (2010). arXiv:1010.3558.
- [45] J. Alwall et al., “MadGraph/MadEvent v4: The New Web Generation”, *JHEP* **09** (2007) 028, doi:10.1088/1126-6708/2007/09/028, arXiv:0706.2334.
- [46] J. M. Campbell and R. K. Ellis, “ $t\bar{t}W^\pm$ production and decay at NLO”, *JHEP* **1207** (2012) 052, doi:10.1007/JHEP07(2012)052, arXiv:1204.5678.
- [47] “Search for electroweak production of charginos and neutralinos in final states with a Higgs boson in pp collisions at $\sqrt{s} = 8$ TeV”, Technical Report CMS-PAS-SUS-13-017, CERN, Geneva, (2013).
- [48] CMS Collaboration, “Search for heavy narrow dilepton resonances in pp collisions at $\sqrt{s} = 7$ TeV and $\sqrt{s} = 8$ TeV”, *Phys.Lett.* **B720** (2013) 63–82, doi:10.1016/j.physletb.2013.02.003, arXiv:1212.6175.
- [49] CMS Collaboration, “CMS technical design report, volume II: Physics performance”, *J.Phys.* **G34** (2007) 995–1579, doi:10.1088/0954-3899/34/6/S01.

- [50] Y. Li and F. Petriello, “Combining QCD and electroweak corrections to dilepton production in FEWZ”, *Phys.Rev.* **D86** (2012) 094034,
[doi:10.1103/PhysRevD.86.094034](https://doi.org/10.1103/PhysRevD.86.094034), arXiv:1208.5967.
- [51] G. Altarelli, B. Mele, and M. Ruiz-Altaba, “Searching for new heavy vector bosons in p anti-p colliders”, *Z.Phys.* **C45** (1989) 109,
[doi:10.1007/BF01552335](https://doi.org/10.1007/BF01552335), [10.1007/BF01556677](https://doi.org/10.1007/BF01556677).
- [52] Y. Bai and T. M. Tait, “Searches with Mono-Leptons”, *Phys.Lett.* **B723** (2013) 384–387,
[doi:10.1016/j.physletb.2013.05.057](https://doi.org/10.1016/j.physletb.2013.05.057), arXiv:1208.4361.
- [53] J. Goodman et al., “Constraints on Dark Matter from Colliders”, *Phys.Rev.* **D82** (2010) 116010, [doi:10.1103/PhysRevD.82.116010](https://doi.org/10.1103/PhysRevD.82.116010), arXiv:1008.1783.
- [54] CMS Collaboration, “Search for new physics in the final states with a lepton and missing transverse energy at $\sqrt{s}=8$ TeV”, CMS Physics Analysis Summary CMS-PAS-EXO-12-060, (2013).
- [55] CMS Collaboration, “Mono-lepton dark matter interpretation at $\sqrt{s} = 8$ TeV”, CMS Physics Analysis Summary CMS-PAS-EXO-13-004, (2013).
- [56] CMS Collaboration, “Searches for long-lived charged particles in pp collisions at $\sqrt{s}=7$ and 8 TeV”, arXiv:1305.0491.
- [57] CMS Collaboration, “Search for Heavy Stable Charged Particles with 100 inverse picobarns and 1 inverse femtobarn in the CMS experiment”, Technical Report CMS-PAS-EXO-08-003, (2009).
- [58] N. Arkani-Hamed, A. G. Cohen, and H. Georgi, “Electroweak symmetry breaking from dimensional deconstruction”, *Phys.Lett.* **B513** (2001) 232–240,
[doi:10.1016/S0370-2693\(01\)00741-9](https://doi.org/10.1016/S0370-2693(01)00741-9), arXiv:hep-ph/0105239.
- [59] M. Schmaltz and D. Tucker-Smith, “Little Higgs Theories”, *Ann.Rev.Nucl.Part.Sci.* **55** (2005) 229–270, [doi:10.1146/annurev.nucl.55.090704.151502](https://doi.org/10.1146/annurev.nucl.55.090704.151502), arXiv:hep-ph/0502182.
- [60] F. del Aguila, L. Ametller, G. L. Kane, and J. Vidal, “Vector-like fermion and standard Higgs production at hadron colliders”, *Nucl.Phys.* **B334** (1990) 1,
[doi:10.1016/0550-3213\(90\)90655-W](https://doi.org/10.1016/0550-3213(90)90655-W).
- [61] CMS Collaboration, “Inclusive search for a vector-like T quark by CMS”, Technical Report CMS-PAS-B2G-12-015, (2013).
- [62] M. Czakon, P. Fiedler, and A. Mitov, “The total top quark pair production cross-section at hadron colliders through $\mathcal{O}(\alpha_S^4)$ ”, (2013). arXiv:1303.6254.
- [63] CMS Collaboration, “Measurement of differential top-quark pair production cross sections in pp collisions at $\sqrt{s} = 7$ TeV”, *Eur. Phys. J. C* **73** (2013) 2339,
[doi:10.1140/epjc/s10052-013-2339-4](https://doi.org/10.1140/epjc/s10052-013-2339-4).
- [64] CMS Collaboration, “Measurement of the differential ttbar cross section in the dilepton channel at 8 TeV”, CMS Physics Analysis Summary CMS-PAS-TOP-12-028, (2013).
- [65] J. A. Aguilar-Saavedra, “Top flavor-changing neutral coupling signals at a linear collider”, *Phys. Lett. B* **502** (2001) 115, [doi:10.1016/S0370-2693\(01\)00162-9](https://doi.org/10.1016/S0370-2693(01)00162-9), arXiv:hep-ph/0012305.

- [66] G. Lu et al., “Rare top quark decays t to cV in the topcolor assisted technicolor model”, *Phys. Rev. D* **68** (2003) 015002, doi:10.1103/PhysRevD.68.015002, arXiv:hep-ph/0303122.
- [67] CMS Collaboration, “Search for flavor-changing neutral currents in top quark decays in pp collisions at 7 TeV”, *Phys. Lett. B* **718** (2012) 1252, doi:10.1016/j.physletb.2012.12.045.
- [68] J. M. Yang, B.-L. Young, and X. Zhang, “Flavor-changing top decays in R parity violating SUSY”, *Phys. Rev. D* **58** (1998) 055001, doi:10.1103/PhysRevD.58.055001.
- [69] C. Zhang and W. S., “Effective-field-theory approach to top-quark production and decays”, *Phys. Rev. D* **83** (2011) 034006, doi:10.1103/PhysRevD.83.034006.
- [70] CMS Collaboration, “Measurement of associated production of vector bosons and top quark-antiquark pairs in pp collisions at $\sqrt{s} = 7$ TeV”, *Phys. Rev. Lett.* **110** (2013) 172002, doi:10.1103/PhysRevLett.110.172002.
- [71] D. Krohn, T. Liu, J. Shelton, and L.-T. Wang, “A Polarized View of the Top Asymmetry”, *Phys. Rev. D* **84** (2011) 074034, doi:10.1103/PhysRevD.84.074034, arXiv:1105.3743.
- [72] W. Bernreuther and Z.-G. Si, “Distributions and correlations for top quark pair production and decay at the Tevatron and LHC”, *Nuc. Phys. B* **837** (2010) 90, doi:10.1016/j.nuclphysb.2010.05.001, arXiv:1003.3926.
- [73] J. A. Aguilar-Saavedra and A. Juste, “A collider independent $t\bar{t}$ forward backward asymmetry”, *Phys. Rev. Lett.* **109** (2012) 211804, doi:10.1103/PhysRevLett.109.211804, arXiv:1205.1898.
- [74] CMS Collaboration, “Measurement of the top-quark mass using the B-hadron lifetime technique”, CMS Physics Analysis Summary CMS-PAS-TOP-12-030, (2013).
- [75] CMS Collaboration, “Study of the dependence of the top-quark mass measurement on event kinematics”, CMS Physics Analysis Summary CMS-PAS-TOP-12-029, (2012).
- [76] CMS Collaboration, “Measurement of the mass difference between top and antitop quarks”, *J. High Energy Phys.* **06** (2012) 109, doi:10.1007/JHEP06(2012)109.
- [77] CMS Collaboration, “Measurement of the top - antitop mass difference in pp collisions at $\sqrt{s} = 8$ TeV”, CMS Physics Analysis Summary CMS-PAS-TOP-12-031, (2013).
- [78] CMS Collaboration, “Study of exclusive two-photon production of W^+W^- in pp collisions at $\sqrt{s} = 7$ TeV and constraints on anomalous quartic gauge couplings”, *JHEP* **1307** (2013) 116, doi:10.1007/JHEP07(2013)116, arXiv:1305.5596.
- [79] CMS Collaboration, “Measurement of the hadronic activity in events with a Z and two jets and extraction of the cross section for the electroweak production of a Z with two jets in pp collisions at $\sqrt{s} = 7$ TeV”, arXiv:1305.7389.
- [80] CMS Collaboration, “Measurement of the weak mixing angle with the Drell-Yan process in proton-proton collisions at the LHC”, *Phys. Rev. D* **84** (2011) 112002, doi:10.1103/PhysRevD.84.112002, arXiv:1110.2682.

- [81] CMS Collaboration, "Measurement of associated charm production in W final states at $\sqrt{s} = 7$ TeV", CMS Physics Analysis Summary CMS-PAS-SMP-12-002, (2013).
- [82] CMS Collaboration, "Measurement of the electron charge asymmetry in inclusive W production in pp collisions at $\sqrt{s} = 7$ TeV", *Phys.Rev.Lett.* **109** (2012) 111806,
`doi:10.1103/PhysRevLett.109.111806`, `arXiv:1206.2598`.
- [83] CMS Collaboration, "Muon charge asymmetry in inclusive W production at 7 TeV", CMS Physics Analysis Summary CMS-PAS-SMP-12-021, (2013).
- [84] CMS Collaboration, "Observation and studies of jet quenching in PbPb collisions at nucleon-nucleon center-of-mass energy = 2.76 TeV", *Phys.Rev.* **C84** (2011) 024906,
`doi:10.1103/PhysRevC.84.024906`, `arXiv:1102.1957`.
- [85] CMS Collaboration, "Jet momentum dependence of jet quenching in PbPb collisions at $\sqrt{s_{NN}} = 2.76$ TeV", *Phys.Lett.* **B712** (2012) 176–197,
`doi:10.1016/j.physletb.2012.04.058`, `arXiv:1202.5022`.
- [86] CMS Collaboration, "Studies of jet quenching using isolated-photon+jet correlations in PbPb and pp collisions at $\sqrt{s_{NN}} = 2.76$ TeV", *Phys.Lett.* **B718** (2013) 773–794,
`doi:10.1016/j.physletb.2012.11.003`, `arXiv:1205.0206`.